J. Fluid Mech. (2021), *vol*. 918, A32, doi:10.1017/jfm.2021.278

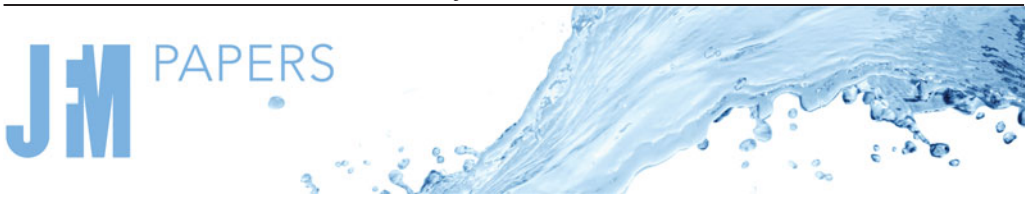

Analytical solutions for one-dimensional diabatic flows with wall friction

Alessandro Ferrari†

Energy Department, Politecnico di Torino, Corso Duca degli Abruzzi 24, Torino 10129, Italy

(Received 3 October 2020; revised 9 March 2021; accepted 22 March 2021)

New analytical solutions for the one-dimensional (1-D) steady-state compressible viscous diabatic flow of an ideal gas through a constant cross-section pipe have been obtained. A constant and a variable heat flux with the walls, the latter being the more relevant for engineering applications, have been considered. To be able to analytically solve the problem, it is essential to determine the correct transformations of the variables and to identify the kinetic energy per unit of mass as the physical variable that appears in the final ordinary differential equation. A dimensionless representation of the analytical solutions, which points out the fundamental role exerted by a few dimensionless groups in problems where viscous power dissipation and heat transfer power are present simultaneously, is also presented. The obtained analytical solutions have successfully been validated for both subsonic and supersonic flows through a comparison with the corresponding numerical time asymptotic solutions of the generalised Euler equations for 1-D gas dynamics problems. The thus validated analytical solutions, which have also been physically discussed, extend Fanno's (1904) and Rayleigh's (1910) models that refer to 1-D steady-state viscous adiabatic and inviscid diabatic flows, respectively.

Key words: high-speed flow, general fluid mechanics, gas dynamics

1. Introduction

Ducts play an important role in engineering simulations: their models can be applied to many thermodynamic systems, such as heat exchangers and refrigeration systems, gas transport systems, gas turbines, wind tunnels, internal combustion engines and aerospace propulsion systems (Maicke & Majdalani 2012; Rodriguez Lastra *et al.* 2013; Cavazzuti & Corticelli 2017).

In general, only numerical solutions can be provided for unsteady or multidimensional steady-state thermofluid dynamics problems involving pipes, once the appropriate initial and boundary conditions have been assigned. However, if the motion is laminar and is

† Email address for correspondence: alessandro.ferrari@polito.it

characterised by lower Mach numbers than 0.3, the fluid can be treated as incompressible (Emmons 1958), and exact solutions can be obtained for two-dimensional steady-state flows in ducts. In fact, in such a case, provided the dynamic viscosity of the fluid can be treated as being independent of the temperature (a feasible hypothesis for gases), Navier–Stokes continuity and momentum balance equations can be solved separately from the energy equation (Batchelor 2000).

If a duct features regular and symmetrical cross-section shapes, negligible curvature of the axis and a sufficiently high aspect ratio, a one-dimensional (1-D) approach can be adopted for the space distribution of the flow properties over the pipe, and generalised Euler equations can be applied to both laminar and turbulent regimes (Douglas *et al.* 2005; White 2015). One-dimensional steady-state models of ducts are popular in the engineering communities that deal with aerospace propulsion (Sutton 1992; Yu *et al.* 2020), power generation equipment (Maicke & Majdalani 2012) and computational fluid dynamics (Toro 2009). Although 1-D approaches are simplified, because no boundary layer is simulated and the turbulent viscous effects can only be modelled roughly using the wall friction approach and the Moody diagram (Douglas *et al.* 2005; White 2015), their surprising simplicity has them to be widely accepted in both academic and industrial circles.

When the kinetic energy of a flow is significant and cannot be disregarded, as typically occurs in the gas dynamics field, there are only a few known cases for which a 1-D steady-state flow along a duct can admit an exact solution.

If the heat transfer flux is negligible and the flow occurs along a constant cross-section pipe with wall friction, the exact solution can be expressed using Fanno's analytical model (1904), which was originally used for subsonic flows and then extended to supersonic flows (Kirkland 2019). Instead, if the heat transfer is significant (the heat flux can be either a constant value or a function of the fluid temperature, according to a convective model), friction is negligible and the flow occurs along a constant cross-section pipe, the Rayleigh model (1910) can be used to determine the exact solution (Anderson 2003).

The above-mentioned exact models only take into account a single flow variation effect, that is, friction or heat transfer, and, for this reason, they fall within the class of simple flows (Shapiro 1953). Because of their importance, these two models have also been extended to include the simulation of elements, such as orifices, elbows and bends (Morimune, Hirayama & Maeda 1980*a*), or sudden cross-section enlargements (Morimune, Hirayama & Maeda 1980*b*). This is obtained by including semi-empirical factors or relations, determined with the support of experimental tests, in the 1-D theoretical models used for a constant cross-section pipe.

Shapiro, going beyond simple flows, determined an exact solution for the 1-D steady-state modelling of both friction and heat transfer effects along a constant cross-section pipe, but assuming an isothermal flow (Shapiro 1953). The more general case of a viscous diabatic flow, without the assumption of barotropic evolution (Prud'homme 2010), is not solved in closed form, but only numerically (Cavazzuti, Corticelli & Karayiannis 2020). On a broader spectrum, no analytical solutions exist, in the gas dynamics field, for flows with more than one single factor driving the fluid property changes (the third factor, in addition to friction or heat transfer, may be a gradual variation of the cross-section pipe), except for a recent exact solution that was determined for the case of a conical nozzle with wall friction (Ferrari 2021).

The objective of the present paper is to physically analyse and analytically solve compressible flows that include both wall friction and heat transfer effects in the presence of significant kinetic energy. The provided steady-state solutions to the Euler equations extend the collection of analytical solutions of gas dynamics and may be

valuable for the validation of numerical models or for providing feasible initial data for transient flow simulations. Furthermore, they can be used for design and control purposes in many technological applications, such as micro- and mini-scale flows (Rosa, Karayiannis & Collins 2009), heat exchangers and refrigeration circuits (Kumar & Ooi 2014), bioengineering and nuclear industry systems (Mignot, Anderson & Corradini 2009). The interest in micro- and mini-scale flows has constantly been increasing in recent years, thanks to the resort to miniaturisation in many technological fields (Rosa *et al.* 2009). Because of their large specific surfaces, mini- and micro-channels are dominated by surface friction (Cioncolini *et al.* 2016) and can require high heat fluxes (Kandlikar *et al.* 2013). When the involved fluid is a gas, this translates into abrupt accelerations and high velocities, therefore fluid compressibility and kinetic energy cannot be neglected (Cavazzuti *et al.* 2020).

2. One-dimensional approach for diabatic flows with friction

Generalised Euler partial differential equations (PDEs) for a 1-D unsteady viscous diabatic gaseous flow along a pipe with constant circular cross-section are given by (Bermudez, Lopez & Vasquez-Cendon 2017)

$$\left.\begin{aligned} \frac{\partial \rho}{\partial t} + \frac{\partial (\rho u)}{\partial x} &= 0 \\ \frac{\partial (\rho u)}{\partial t} + \frac{\partial (p + \rho u^2)}{\partial x} &= -\frac{4\tau_w}{D} \\ \frac{\partial (\rho e^0)}{\partial t} + \frac{\partial (\rho u h^0)}{\partial x} &= \frac{4\dot{q}_f}{D} \end{aligned}\right\}, \tag{2.1}$$

where t is the time, x is the space coordinate, ρ, u and p are the cross-section averaged 1-D density, velocity and pressure, respectively, D is the pipe diameter ($A = \pi/4D^2$ is the cross-section), e^0 is the stagnation internal energy ($e^0 = e + u^2/2$, where e is the internal energy), h^0 is the stagnation enthalpy ($h^0 = h + u^2/2$, where h is the enthalpy), τ_w is the wall friction shear stress and $\dot{q}_f$ is the heat flux exchanged by the fluid with the walls ($\dot{q}_f$ is positive when the heat is supplied to the fluid).

Equation (2.1) differs from the standard set of Euler equations for an isentropic flow because the friction and heat exchange are added and evaluated as volume source terms (Hirsch 2007; Maeda & Colonius 2017), using the Darcy–Weisbach wall friction and convective heat transfer models. The wall friction stress is expressed by (White 2015)

$$\tau_w = \frac{f}{2}\rho u|u|, \tag{2.2}$$

where the friction coefficient f can be expressed as a function of the Reynolds number ($Re = \rho u D/\mu$, with μ being the dynamical viscosity of the fluid) for a laminar flow and as a function of both Re and the relative roughness (ϵ/D, with ϵ being the average roughness of the wall) for a turbulent flow (Douglas *et al.* 2005; Cheng 2008; White 2015). The heat flux can be expressed as (Bejan 2013)

$$\dot{q}_f = \lambda(T_w - T), \tag{2.3}$$

where the film coefficient λ [W (m^2 K)$^{-1}$] is a function of the Reynolds and Prandtl (Pr) numbers, T is the cross-section averaged 1-D temperature of the fluid and T_w is the uniform wall temperature.

Equations (2.1)–(2.3) are completed with the following state equations of the gas:

$$\left.\begin{aligned} p &= \frac{\gamma-1}{\gamma}\rho h, \quad h = c_p T \\ h &= e + \frac{p}{\rho}, \quad e = c_v T \end{aligned}\right\}, \tag{2.4}$$

where $\gamma = c_p/c_v$ is the ratio of the constant pressure specific heat (c_p) to the constant volume specific heat (c_v).

When steady-state flows are considered, the partial derivatives with respect to time vanish in (2.1), which can be reduced to the following system of nonlinear ordinary differential equations (ODEs) with respect to the independent variable x (Emmons 1958):

$$\left.\begin{aligned} \frac{\mathrm{d}\dot{m}}{\mathrm{d}x} &= 0 \\ A\frac{\mathrm{d}p}{\mathrm{d}x} + \dot{m}\frac{\mathrm{d}u}{\mathrm{d}x} &= -\pi D\tau_w \\ \dot{m}\frac{\mathrm{d}h^0}{\mathrm{d}x} &= \pi D\dot{q}_f \end{aligned}\right\}, \tag{2.5}$$

where $\dot{m} = \rho A u$ is the mass flow rate through the pipe.

3. Exact 1-D solution for steady-state compressible viscous flows with constant $\dot{q}_f$

Let us consider a steady-state compressible viscous diabatic flow with constant $\dot{q}_f$ along a constant circular cross-section pipe. The mass conservation law in (2.5) can be rewritten as

$$\rho u = \frac{\dot{m}}{A} = \text{const} \tag{3.1}$$

Furthermore, the momentum balance and total energy laws in (2.5) can be rearranged as follows (the momentum balance and total energy equations are divided by $A\rho$ and A, respectively, and (2.2) is used with $u > 0$):

$$\frac{4f}{D}\left(\frac{u^2}{2}\right) + \frac{A}{\dot{m}}u\frac{\mathrm{d}p}{\mathrm{d}x} + \frac{\mathrm{d}}{\mathrm{d}x}\left(\frac{u^2}{2}\right) = 0, \tag{3.2}$$

$$\frac{\dot{m}}{A}\frac{\mathrm{d}h}{\mathrm{d}x} + \frac{\dot{m}}{A}\frac{\mathrm{d}}{\mathrm{d}x}\left(\frac{u^2}{2}\right) = \frac{4\dot{q}_f}{D}, \tag{3.3}$$

where f is a constant term, because $Re = \rho u D/\mu = 4\dot{m}/(\pi D\mu) = \text{const}$ (the dependence of the dynamic viscosity of the fluid on T is neglected). The pressure can be expressed according to the following formula, which was obtained using the state equations of ideal gases, i.e. (2.4), in conjunction with (3.1):

$$p = \frac{\gamma-1}{\gamma}\rho h = \frac{\gamma-1}{\gamma}\frac{\dot{m}}{Au}h. \tag{3.4}$$

Therefore, the pressure gradient can be calculated by applying the chain rule:

$$\frac{\mathrm{d}p}{\mathrm{d}x} = \frac{\dot{m}}{Au}\frac{\gamma-1}{\gamma}\frac{\mathrm{d}h}{\mathrm{d}x} - \frac{\dot{m}}{Au^2}\frac{\gamma-1}{\gamma}h\frac{\mathrm{d}u}{\mathrm{d}x}. \tag{3.5}$$

By substituting (3.5) in (3.2) and taking (3.3) into account, we obtain

$$\frac{4f}{D}\left(\frac{u^2}{2}\right)-\frac{\gamma-1}{2\gamma}h\frac{\mathrm{d}}{\mathrm{d}x}\left[\ln\left(\frac{u^2}{2}\right)\right]-\frac{1}{\gamma}\frac{\mathrm{d}h}{\mathrm{d}x}=-\frac{\dot{q}_f\pi D}{\dot{m}}. \tag{3.6}$$

Equation (3.3) can be divided by $\dot{m}/A$ and, because $\dot{q}_f$ is supposed to be a constant term ($\dot{q}_f$ can be either positive or negative), it can easily be integrated with respect to x to obtain

$$h=h_1^0+\frac{\dot{q}_f\pi D}{\dot{m}}x-\frac{u^2}{2}, \tag{3.7}$$

where h_1^0 is the stagnation enthalpy at $x_1=0$ ($h_1^0=c_pT_1^0$). Equation (3.7) can then be used to eliminate h from (3.6) and, after some analytical steps, the following equation can be achieved:

$$\frac{4f}{D}\left(\frac{u^2}{2}\right)-\frac{\gamma-1}{2\gamma}\left(h_1^0+\frac{\dot{q}_f\pi Dx}{\dot{m}}\right)\frac{\mathrm{d}}{\mathrm{d}x}\left[\ln\left(\frac{u^2}{2}\right)\right]+\frac{\gamma+1}{2\gamma}\frac{\mathrm{d}}{\mathrm{d}x}\left(\frac{u^2}{2}\right)=\frac{1-\gamma}{\gamma}\frac{\dot{q}_f\pi D}{\dot{m}}. \tag{3.8}$$

Equation (3.8) is a nonlinear ODE with a single unknown function, that is, the kinetic energy per unit of mass ($u^2/2$). By changing the variable (let us use the letter 't' for the new variable because there is no time in the rest of the current section)

$$t:=\ln\left(\frac{u^2}{2}\right), \tag{3.9}$$

and performing some algebraic manipulation, (3.8) can finally be converted into the following heterogeneous linear ODE:

$$\frac{\mathrm{d}x}{\mathrm{d}t}+a(t)x=b(t), \tag{3.10}$$

where

$$a(t)=-\left(\frac{\dfrac{\gamma-1}{2\gamma}\dfrac{\dot{q}_f\pi D}{\dot{m}}}{\dfrac{4f}{D}e^t+\dfrac{\gamma-1}{\gamma}\dfrac{\dot{q}_f\pi D}{\dot{m}}}\right)\qquad b(t)=\left(\frac{\dfrac{\gamma-1}{2\gamma}h_1^0-\dfrac{\gamma+1}{2\gamma}e^t}{\dfrac{4f}{D}e^t+\dfrac{\gamma-1}{\gamma}\dfrac{\dot{q}_f\pi D}{\dot{m}}}\right). \tag{3.11}$$

It is known that any linear first-order ODE with variable coefficients can be solved using Lagrange's method of variation of the constants (Hairer, Norsett & Wanner 1993). The general solution to (3.10) takes the form

$$x(t)=\mathrm{e}^{-A(t)}\left[\int b(t)\,\mathrm{e}^{A(t)}+C\right], \tag{3.12}$$

where $A(t)=\int a(t)\,\mathrm{d}t$ is a primitive function of $a(t)$ and C is a constant value that can be calculated by assigning a boundary condition to the Cauchy problem.

By using the above expression for $a(t)$, one obtains (the integral $\int a(t)\,\mathrm{d}t$ is of the form $-1/2\int B/(\mathrm{e}^t+B)\,\mathrm{d}t = 1/2\ln(|e^t+B|/e^t)$, where B is a general constant term)

$$A(t) = -\int\left(\frac{\dfrac{\gamma-1}{2\gamma}\dfrac{\dot{q}_f\pi D}{\dot{m}}}{\dfrac{4f}{D}e^t+\dfrac{\gamma-1}{\gamma}\dfrac{\dot{q}_f\pi D}{\dot{m}}}\right)\mathrm{d}t = \ln\frac{\left|\mathrm{e}^t+\dfrac{\gamma-1}{\gamma}\dfrac{\dot{q}_f\pi D^2}{4f\dot{m}}\right|^{1/2}}{\mathrm{e}^{t/2}}, \tag{3.13}$$

and consequently (3.12), after some algebraic manipulation and recalling that $t = \ln(u^2/2)$, becomes

$$x = \left\{sgn\left(\frac{u^2}{2}+\frac{\gamma-1}{\gamma}\frac{\dot{q}_f\pi D^2}{4f\dot{m}}\right)\int\left[\frac{\dfrac{\gamma-1}{\gamma}\dfrac{D}{8f}h_1^0-\dfrac{\gamma+1}{\gamma}\dfrac{D}{8f}\dfrac{u^2}{2}}{\left(\dfrac{u^2}{2}\right)^{3/2}\left|\dfrac{u^2}{2}+\dfrac{\gamma-1}{\gamma}\dfrac{\dot{q}_f\pi D^2}{4f\dot{m}}\right|^{1/2}}\right]d\left(\frac{u^2}{2}\right)+C\right\}$$
$$\times\frac{\left(\dfrac{u^2}{2}\right)^{1/2}}{\left|\dfrac{u^2}{2}+\dfrac{\gamma-1}{\gamma}\dfrac{\dot{q}_f\pi D^2}{4f\dot{m}}\right|^{1/2}}, \tag{3.14}$$

where *sgn* represents the signum function, which extracts the sign of the quantity to which it is applied. The indefinite integral should be resolved to obtain an effective solution to the fluid dynamics problem in closed form. As a result of the change in variable $w = \sqrt{u^2/2}$, one obtains

$$\int\left[\frac{\dfrac{\gamma-1}{\gamma}\dfrac{D}{8f}h_1^0-\dfrac{\gamma+1}{\gamma}\dfrac{D}{8f}\dfrac{u^2}{2}}{\left|\dfrac{u^2}{2}+\dfrac{\gamma-1}{\gamma}\dfrac{\dot{q}_f\pi D^2}{4f\dot{m}}\right|^{1/2}\left(\dfrac{u^2}{2}\right)^{3/2}}\right]d\left(\frac{u^2}{2}\right) = \int\left[\frac{\dfrac{\gamma-1}{\gamma}\dfrac{D}{4f}h_1^0-\dfrac{\gamma+1}{\gamma}\dfrac{D}{4f}w^2}{w^2\left|w^2+\dfrac{\gamma-1}{\gamma}\dfrac{\dot{q}_f\pi D^2}{4f\dot{m}}\right|^{1/2}}\right]\mathrm{d}w. \tag{3.15}$$

The indefinite integral on the right-hand side of (3.15) can be interpreted as

$$\int\left[\frac{\dfrac{\gamma-1}{\gamma}\dfrac{D}{4f}h_1^0-\dfrac{\gamma+1}{\gamma}\dfrac{D}{4f}w^2}{w^2\left|w^2+\dfrac{\gamma-1}{\gamma}\dfrac{\dot{q}_f\pi D^2}{4f\dot{m}}\right|^{1/2}}\right]\mathrm{d}w \Rightarrow \int\left[\frac{F-Gw^2}{w^2\sqrt{|w^2+E|}}\right]\mathrm{d}w$$
$$= \int\left[\frac{F}{w^2\sqrt{|w^2+E|}}-\frac{G}{\sqrt{|w^2+E|}}\right]\mathrm{d}w, \tag{3.16}$$

where $E = (\gamma-1)\dot{q}_f\pi D^2/(4\gamma f\dot{m})$, $F = (\gamma-1)Dh_1^0/(4\gamma f)$ and $G = (\gamma+1)D/(4\gamma f)$ are constant terms in the considered problem, that is, they are independent of w.

Let us suppose that $w^2 + E > 0 \,\forall x$ ($\dot{q}_f$ can still be either positive or negative with this hypothesis). The initial integral in (3.16) is split into two indefinite integrals that can be expressed in terms of the following elementary functions (Dwight 1961):

$$\left.\begin{aligned} \int \frac{G}{\sqrt{w^2+E}}\,\mathrm{d}w &= G\ln\frac{w+\sqrt{w^2+E}}{\sqrt{|E|}} \\ \int \frac{F}{w^2\sqrt{w^2+E}}\,\mathrm{d}w &= -\frac{F}{E}\frac{\sqrt{w^2+E}}{w} \end{aligned}\right\}. \tag{3.17}$$

By considering (3.14)–(3.17), the general analytical solution to (3.8) is provided explicitly as $x = x(u^2/2)$:

$$x = -\frac{\dot{m}h_1^0}{\dot{q}_f \pi D} + \left\{ C - \frac{\gamma+1}{\gamma}\frac{D}{4f}\ln\left[\frac{\sqrt{\dfrac{u^2}{2}} + \sqrt{\dfrac{u^2}{2} + \dfrac{\gamma-1}{\gamma}\dfrac{\dot{q}_f \pi D^2}{4f\dot{m}}}}{\sqrt{\dfrac{\gamma-1}{\gamma}\dfrac{|\dot{q}_f|\pi D^2}{4f\dot{m}}}}\right]\right\} \frac{\sqrt{\dfrac{u^2}{2}}}{\sqrt{\dfrac{u^2}{2} + \dfrac{\gamma-1}{\gamma}\dfrac{\dot{q}_f \pi D^2}{4f\dot{m}}}}. \tag{3.18}$$

Once the value of integration constant C has been determined (cf. § 3.1), (3.18) becomes well defined. The 1-D T versus x distribution can then be expressed in parametric form using (3.7) and (3.18), where the kinetic energy per unit of mass of the fluid is the parameter:

$$\left.\begin{aligned} T &= T_1^0 + \frac{\dot{q}_f \pi D}{\dot{m} c_p} x\left(\frac{u^2}{2}\right) - \frac{u^2}{2c_p} \\ x &= x\left(\frac{u^2}{2}\right) \end{aligned}\right\}. \tag{3.19}$$

Furthermore, the density and pressure distributions, with respect to x, can be expressed as parametric equations: $\rho(x)$ is obtained by coupling (3.18) with (3.1) and $p(x)$ is achieved by linking (3.18) with both (3.4) and (3.7).

Finally, the Mach number distributions with respect to x can also be determined in parametric form by using (3.18) and (3.19) as well as the formula $Ma = \sqrt{u^2/(\gamma RT)}$.

The exact solutions and the corresponding analytical variants for the $w^2 + E = 0$ and $w^2 + E < 0$ cases are discussed in the appendix of the paper to avoid excessive fragmentation of the theoretical development with the introduction of too many details. Although these cases are essential to complete the exact solution, the main objective of the present paper is to highlight a methodology that can be used for the analytical treatment and physical interpretation of compressible viscous diabatic flows. It therefore appeared more efficient to present the procedure by only making preliminarily reference to the $w^2 + E > 0 \,\forall x$ condition and then extending the method to the other cases in the appendix.

3.1. *Input data for the physical problem and determination of constant C*

The constant heat flux is regarded as a given value in the present approach. In fact, the heat transfer power $\dot{Q}$ (either positive or negative), exchanged entirely through the walls of the circular pipe of assigned length L and diameter D, should be provided as an input

value for the physical problem, and the heat flux per unit of area can thus be defined using the formula $\dot{q}_f = \dot{Q}/(\pi DL)$.

Furthermore, three independent boundary conditions are required to determine the values of the constant terms h_1^0, $\dot{m}$ and C in (3.18). These three boundary conditions, for the numerical solution of the unsteady PDE problem given by (2.1)–(2.3), should be provided following precise rules, according to the characteristic theory of systems of hyperbolic partial differential equations (Toro 2009).

It is not necessary to pursue this theory in the present case because a steady-state problem is being analysed. In fact, the three input data values can be assigned at the $x_1 = 0$ and $x_2 = L$ boundaries, without any constraints (Urata 2013), although the easiest choice is to provide the mass flow rate and total temperature as well as the fluid velocity at the inlet of the pipe ($x_1 = 0$). However, we here follow the characteristic line approach because it is exhaustive in illustrating how the available data at the boundaries can be used to determine the analytical solution.

According to the characteristic line theory, when the flow through the pipe is subsonic, two boundary conditions should be assigned at the pipe inlet, namely T_1^0 and total pressure (p_1^0), while one boundary datum should be provided at the pipe exit ($x_2 = L$), namely the static pressure (p_V) of the pipe downstream environment.

A shooting procedure can therefore be arranged: a tentative value of Ma_1 can be selected, and $u_1^2/2$ and $\dot{m}$ can then be determined using the following equations, which refer to an isentropic evolution from the stagnation conditions to state 1 (Zucker & Biblarz 2002):

$$\left.\begin{aligned} \frac{u_1^2}{2} &= c_p T_1^0 Ma_1^2 \left(\frac{2}{\gamma - 1} + Ma_1^2\right)^{-1} \\ \dot{m} &= \frac{p_1^0}{\sqrt{RT_1^0}} A\sqrt{\gamma} Ma_1 \left(1 + \frac{\gamma - 1}{2} Ma_1^2\right)^{-(\gamma+1)/2(\gamma-1)} \end{aligned}\right\}. \tag{3.20}$$

The constant C value can then be calculated by solving (3.18) under the condition $u^2/2 = u_1^2/2$ at $x = x_1 = 0$:

$$C = \frac{\dot{m} h_1^0}{\dot{q}_f \pi D} \frac{\sqrt{\dfrac{u_1^2}{2} + \dfrac{\gamma - 1}{\gamma} \dfrac{\dot{q}_f \pi D^2}{4f\dot{m}}}}{\sqrt{\dfrac{u_1^2}{2}}} + \frac{\gamma + 1}{\gamma} \frac{D}{4f} \ln \left[\frac{\sqrt{\dfrac{u_1^2}{2}} + \sqrt{\dfrac{u_1^2}{2} + \dfrac{\gamma - 1}{\gamma} \dfrac{\dot{q}_f \pi D^2}{4f\dot{m}}}}{\sqrt{\dfrac{\gamma - 1}{\gamma} \dfrac{|\dot{q}_f| \pi D^2}{4f\dot{m}}}} \right]. \tag{3.21}$$

Equation (3.18), with C given by (3.21), can be employed to determine the $u_2^2/2$ at $x_2 = L$ value. Furthermore, density ρ_2 can be evaluated from (3.1), which is applied for $x_2 = L$, and (3.7) can be used to calculate h_2 at $x_2 = L$.

Finally, pressure p_2 can be calculated as a function of ρ_2 and h_2 using (3.4). If the thus determined p_2 value is equal to the provided boundary datum p_V, the guessed value of Ma_1 is suitable, otherwise the shooting procedure should be repeated selecting new values of Ma_1 until consistency with downstream boundary pressure p_V is achieved. At the end of the procedure, C has been evaluated accurately and (3.18) is therefore ready for use. When the flow through the pipe is supersonic, the hyperbolic PDE theory requires that all three boundary conditions are given at the pipe inlet, namely T_1^0, p_1^0 and Ma_1 at $x_1 = 0$.

In this case, both $\dot{m}$ and $u_1^2/2$ can be evaluated directly using (3.20), and C can then be determined using (3.21); hence, (3.18) is completely defined.

3.2. *Dimensionless representation of the exact solution*

Equations (3.18) and (3.21), the physical domain and the required boundary conditions of the problem (for the sake of simplicity, let us here suppose that such boundary conditions are provided by the h_1^0, $\dot{m}$ and $u_1^2/2$ values) involve eight dimensional sizes, that is, x, $\dot{m}$, h_1^0, D, $u^2/2$, $u_1^2/2$, L, $\dot{q}_f$, and two dimensionless parameters, that is, γ and f. Because both mechanical and thermal quantities are involved in the problem, the rank of the dimensional problem is equal to four, i.e. m, s, kg and K are required as measurement units to express all the quantities that appear in the problem.

According to Buckingham's theorem (Yarin 2012), it is possible to express the solution and boundary conditions in terms of $(8+2)-4=6$ dimensionless groups. The dimensionless representation of the solution can be useful to clearly identify the physical factors that drive the analysed phenomenon.

If (3.18) is multiplied by f/D_h, where D_h is the ratio of cross-sectional area to wetted perimeter ($D_h = D/4$ for circular sections), and $\dot{q}_f$ is replaced by the total heat transfer power per unit of mass flow rate, namely q, which is defined as $q = \dot{q}_f \pi DL/\dot{m}$, the following dimensionless equation can be obtained after some algebraic manipulation ($C^* := Cf/D_h$):

$$f\frac{x}{D_h} = -\frac{h_1^0}{q} f\frac{L}{D_h} + \left\{ C^* - \frac{\gamma+1}{\gamma} \ln\left[\frac{\sqrt{\dfrac{u^2}{2|q|}} + \sqrt{\dfrac{u^2}{2|q|} + sgn(\dot{q}_f)\dfrac{\gamma-1}{\gamma}\dfrac{D_h}{fL}}}{\sqrt{\dfrac{\gamma-1}{\gamma}\dfrac{D_h}{fL}}} \right] \right\} \times \frac{\sqrt{\dfrac{u^2}{2|q|}}}{\sqrt{\dfrac{u^2}{2|q|} + sgn(\dot{q}_f)\dfrac{\gamma-1}{\gamma}\dfrac{D_h}{fL}}}. \tag{3.22}$$

Let us now define the following dimensionless number

$$\Pi_L = \frac{\dot{q}_f \pi DL}{\dot{m} h_1^0} = \frac{q}{h_1^0} = \frac{h_2^0 - h_1^0}{h_1^0} = \frac{T_2^0}{T_1^0} - 1, \tag{3.23}$$

which expresses the ratio of the total heat transfer power (over length L of the duct) to the flux of the total enthalpy at the pipe inlet, namely $\dot{m}h_1^0$. When the heat transfer is null, the total enthalpy is conserved along the pipe, hence $\Pi_L = 0$ and Fanno's model is obtained. In general, a higher modulus of Π_L ($\dot{q}_f$ can be either positive or negative) leads to a greater impact of the heat transfer on the flow evolution.

The term $u^2/2|q|$ on the right-hand side of (3.22) can be developed by taking (3.7) and (3.23) into account:

$$\frac{u^2}{2|q|} = \frac{u^2}{2c_p|T_2^0 - T_1^0|} = Cr^2 \frac{T^0/T_1^0}{|T_2^0/T_1^0 - 1|} = \frac{Cr^2}{|\Pi_L|}\left(1 + \Pi_L \frac{x}{L}\right), \tag{3.24}$$

where $Cr = u/\sqrt{2c_pT^0}$ is the Crocco number and T^0 is the stagnation temperature at section x.

By substituting (3.24) and (3.23) in (3.22), and after some algebraic steps, one can obtain the following implicit dimensionless representation of the solution:

$$fx/D_h = -\frac{1}{\Gamma} + \left\{ C^* - \ln\left[\frac{Cr\sqrt{1+\Gamma fx/D_h} + \sqrt{Cr^2(1+\Gamma fx/D_h) + \Gamma^{\frac{\gamma-1}{\gamma}}}}{\sqrt{|\Gamma|^{\frac{\gamma-1}{\gamma}}}} \right]^{(\gamma+1)/\gamma} \right\} \times \frac{Cr\sqrt{1+\Gamma fx/D_h}}{\sqrt{Cr^2(1+\Gamma fx/D_h) + \Gamma^{\frac{\gamma-1}{\gamma}}}}, \tag{3.25}$$

where

$$\Gamma = \frac{\Pi_L}{(fL/D_h)}, \quad C^* = \frac{1}{\Gamma}\frac{\sqrt{Cr_1^2 + \Gamma^{\frac{\gamma-1}{\gamma}}}}{Cr_1} + \ln\left[\frac{Cr_1 + \sqrt{Cr_1^2 + \Gamma^{\frac{\gamma-1}{\gamma}}}}{\sqrt{|\Gamma|^{\frac{\gamma-1}{\gamma}}}} \right]^{(\gamma+1)/\gamma}. \tag{3.26}$$

A practical way of obtaining an explicit dependence of fx/D_h on Cr would be to define the Crocco number as $= u/\sqrt{2c_pT_1^0}$, as is done in some fluid machinery textbooks when the stagnation temperature is variable along the component. However, this is not the preferred choice for theoretical gas dynamics and, above all, the definition of Cr that adopts T_1^0 would not allow fx/D_h to explicitly depend on the Mach number.

Six dimensionless factors appear in (3.25): fx/D_h, Cr, fL/D_h, Π_L, γ and Cr_1 (only fx/D_h and Cr are variable with x, whereas the other factors are fixed parameters of the solution). The Π_L group takes thermal effects into account and is also relevant for a Rayleigh flow, while the fL/D_h and fx/D_h terms, which include the friction coefficient and the aspect ratio of either the pipe or a portion of the pipe, account for the friction effect and are noteworthy groups for Fanno's flow (Shapiro 1953).

Another notable implicit dimensionless representation, which is an alternative to (3.25), is given by

$$\Pi_x = -1 + \left\{ C^* - \ln\left[\frac{Cr\sqrt{1+\Pi_x} + \sqrt{Cr^2(1+\Pi_x) + \Gamma^{\frac{\gamma-1}{\gamma}}}}{\sqrt{|\Gamma|^{\frac{\gamma-1}{\gamma}}}} \right]^{(\gamma+1)/\gamma} \right\} \times \frac{Cr\Gamma\sqrt{1+\Pi_x}}{\sqrt{Cr^2(1+\Pi_x) + \Gamma^{\frac{\gamma-1}{\gamma}}}}, \tag{3.27}$$

where $\Pi_x = \dot{q}_f \pi D x/\dot{m}h_1^0$, and constant C^* has the same expression as that which is valid for (3.25).

The six dimensionless factors in (3.27) are Π_x, Cr, fL/D_h, Π_L, γ and Cr_1. Therefore, variable fx/D_h, which appears in (3.25), has been substituted with variable Π_x in (3.27), on the basis of the $\Pi_x = \Gamma fx/D_h$ relation.

Finally, the Crocco number can be expressed in both (3.25) and (3.27) as a function of γ and the Mach number, according to the formula

$$Cr = \frac{Ma}{\sqrt{Ma^2 + 2/(\gamma - 1)}}. \tag{3.28}$$

Once (3.28) has been substituted in either (3.25) or (3.27), new implicit dimensionless solutions, which link either fx/D_h or Π_x, respectively, to Ma, can be determined for compressible viscous diabatic flows (fL/D_h, Π_L, Ma_1 and γ will be the fixed parameters of the solutions). The advantage of these new dimensionless representations is that they include Ma, which is also a fundamental dimensionless variable in the Fanno and Rayleigh models. This facilitates any comparison between the newly developed analytical model and simple flow analytical models that lead to dimensionless explicit relations between Ma and either fx/D_h (Fanno's model) or Π_x (Rayleigh's model).

The dimensionless representation obtained by coupling (3.25) and (3.28) is suitable for a comparison with the Fanno flow and can therefore be referred to as *Fanno's dimensionless mode representation* of the compressible viscous diabatic flow.

Instead, the dimensionless representation obtained by coupling (3.27) and (3.28) is suitable for comparison with the Rayleigh flow and can be referred to as *Rayleigh's dimensionless mode representation* of the compressible viscous diabatic flow. A fundamental role is played by quantity Γ in both of these representations, which accounts for the relative importance of the heat transfer and friction groups of the whole pipe during the evolution of the viscous diabatic flow.

4. Validation of the exact solutions with constant $\dot{q}_f$

The previously developed analytical solutions were validated through a comparison with the corresponding time asymptotic distributions, which resulted from the numerical solution of (2.1), (2.2) and (2.4). The expression of $\dot{q}_f$ in the PDE numerical model was regarded as a constant value.

The PDEs were discretised using a finite volume method, according to a flux vector splitting technique (Laney 1998; Toro 2009) that applies a high-resolution upwind discretisation scheme with a Van Leer flux limiter (Le Veque 1990). The spatial mesh size, namely Δx, was selected to guarantee a grid independent numerical solution. The time step, namely Δt, was set to obtain $\sigma = 0.9$, where $\sigma = |u + \sqrt{\gamma RT}|_{max}\Delta t/\Delta x$ is the instantaneous Courant number (Tannehill, Anderson & Pletcher 1997) and $|u + \sqrt{\gamma RT}|_{max}$ is the maximum modulus of the $u(x, t) + \sqrt{\gamma RT(x, t)}$ numerical space distribution at each fixed time instant.

The boundary conditions of the PDEs were provided according to the characteristic theory for hyperbolic problems. Therefore, the stagnation temperature and stagnation pressure were assigned to the pipe inlet section for subsonic flows, whereas static pressure was assigned to the pipe downstream environment. Three boundary data, namely stagnation temperature, stagnation pressure and Mach number, were instead assigned to the pipe inlet for supersonic flows, and no boundary data were provided for the pipe exit.

Figures 1 and 2 refer to a steady-state (or time asymptotic for the numerical solution) viscous diabatic flow with a positive constant heat flux ($\dot{q}_f = \text{const} > 0$): figure 1 reports the results of a validation test for a subsonic flow, whereas figure 2 reports the results of a validation test for a supersonic flow.

The analytical solutions are plotted with either a continuous line (velocity) or a dashed line (temperature): the unidimensional diagrams of the velocity were calculated

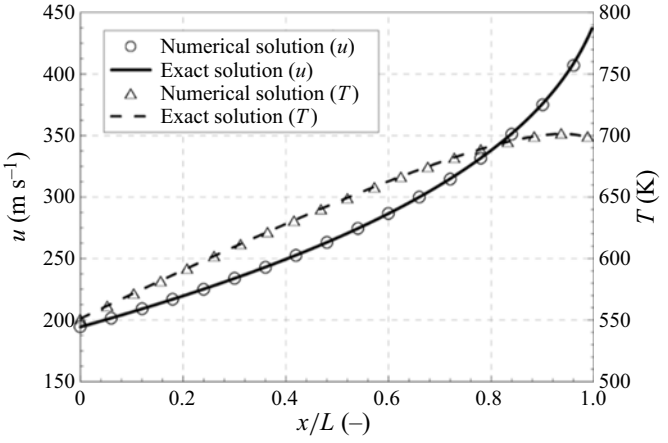

Figure 1. Validation test for the exact solution with a positive constant heat flux for a subsonic flow. Test conditions: $L = 50$ cm, $D = 0.98$ cm, $p_1^0 = 5$ bar, $T_1^0 = 570$ K, $p_V = 2.5$ bar, $f = 4 \times 10^{-3}$, $\dot{q}_f = 6 \times 10^5$ W m^{-2}, $\gamma = 1.4$, $R = 287$ J (kg K)$^{-1}$, $\Delta x = 1$ mm ($\dot{m} = 41.28$ g s^{-1}).

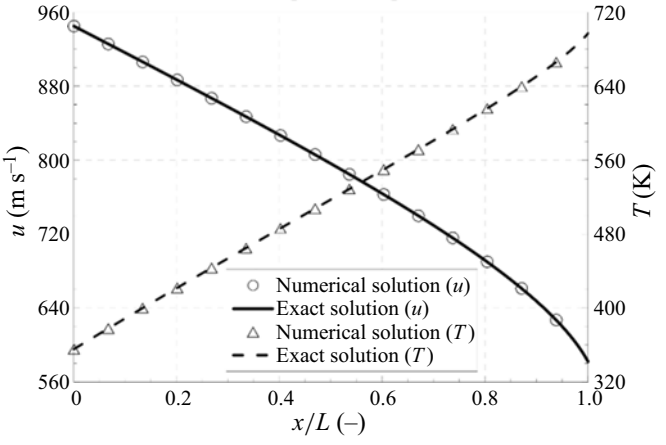

Figure 2. Validation test for the exact solution with a positive constant heat flux for a supersonic flow. Test conditions: $L = 67.16$ cm, $D = 2.5$ cm, $p_1^0 = 3$ bar, $T_1^0 = 800$ K, $Ma_1 = 2.5$, $f = 3 \times 10^{-3}$, $\dot{q}_f = 10^5$ W m^{-2}, $\gamma = 1.4$, $R = 287$ J (kg K)$^{-1}$, $\Delta x = 1$ mm ($\dot{m} = 79.81$ g s^{-1}).

by applying (3.18), whereas the temperature versus x distributions were determined using the parametric relations in (3.19). The numerical solutions are reported with symbols. The constant C in (3.18) was calculated with the shooting procedure illustrated in § 3.1 for the subsonic flow case, whereas C was determined directly, using (3.20) and (3.21), for the supersonic flow case.

Furthermore, figure 3 reports a validation test for a subsonic flow for the case of a negative constant heat flux ($\dot{q}_f = \text{const} < 0, w^2 + E > 0 \,\forall x$) and according to the boundary conditions specified in the caption.

As can be inferred, each graph in figures 1–3 shows an excellent agreement between the corresponding curves, and this is clear proof of the physical consistency of the determined exact solutions for the $\dot{q}_f = \text{const}$ case.

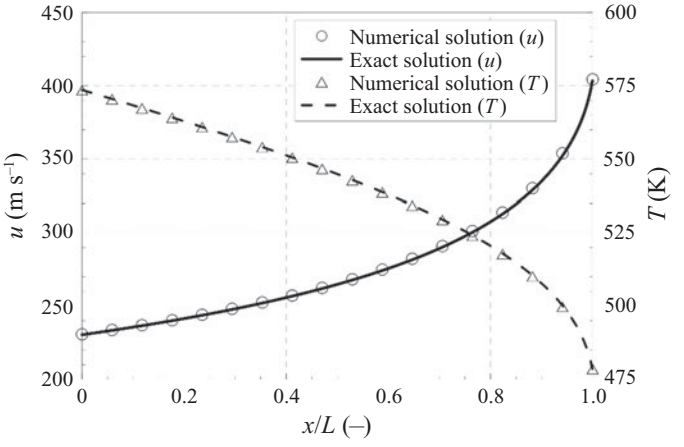

Figure 3. Validation test for the analytical solution with a negative constant heat flux for a subsonic flow. Test conditions: $L = 51$ cm, $D = 0.7$ cm, $p_1^0 = 6$ bar, $T_1^0 = 600$ K, $p_V = 2.44$ bar, $f = 5 \times 10^{-3}$, $\dot{q}_f = -10^5$ W m^{-2}, $\gamma = 1.4$, $R = 287$ J (kg K)$^{-1}$, $\Delta x = 1$ mm ($\dot{m} = 27.6$ g s^{-1}).

5. Physical discussion of the exact solutions with constant $\dot{q}_f$

5.1. *Results in the enthalpy–entropy diagram and identification of choking conditions*

A physical interpretation of the developed exact solutions for compressible viscous diabatic flows in the $\dot{q}_f = \text{const}$ case can be provided by analysing the enthalpy–entropy diagrams, as is usually done when presenting Fanno's and Rayleigh's models.

The h–s curves can be calculated by applying (3.18), (3.19), (3.7) and (3.4), together with the state equation for entropy, that is, $s = c_p \ln(T/T_1^0) - R \ln(p/p_1^0)$, where $s(p_1^0, T_1^0)$ is taken as null.

Figure 4 reports h–s curves that refer to initially subsonic flows for the $\dot{q}_f > 0$ case. All the curves, except that plotted with a dash–dotted line without symbols, are characterised by the same conditions at the pipe inlet (point at $s = 0$), namely T_1^0, p_1^0, D and Ma_1, and thus by the same mass flow rate, which are specified in the caption.

The differences between the curves with the same flow rate arise because different couples of f and $\dot{q}_f$ values have been applied (these values are quoted in the legend). In particular, the continuous solid line without symbols refers to the same T_1^0, p_1^0, $\dot{m}$, f, D and $\dot{q}_f$ conditions as those in the validation test shown in figure 1. The dash–dotted curved line without symbols refers to the same T_1^0, p_1^0, D conditions as those of the other curves and to the same f, $\dot{q}_f$ values as the continuous line without symbols, but features an increased specific flow rate, i.e. a larger value of $\dot{m}/A$ and thus a higher Ma_1.

Figure 5 plots a similar graph to that shown in figure 4, but for supersonic viscous diabatic flows: the curve plotted with a continuous line without any symbols refers to the same T_1^0, p_1^0, $\dot{m}$, f, D and $\dot{q}_f$ conditions as in the validation test of figure 2. The f and positive $\dot{q}_f$ values pertaining to the other curves plotted with symbols, which refer to the same T_1^0, p_1^0, D and $\dot{m}$ conditions as those for the continuous curve without symbols, are also reported in the legend. Furthermore, a portion of the curve that refers to a larger value of $\dot{m}/A$ has been reported with a dash–dotted line to show the effect of an increased specific flow rate on the h-s curves, as in figure 4.

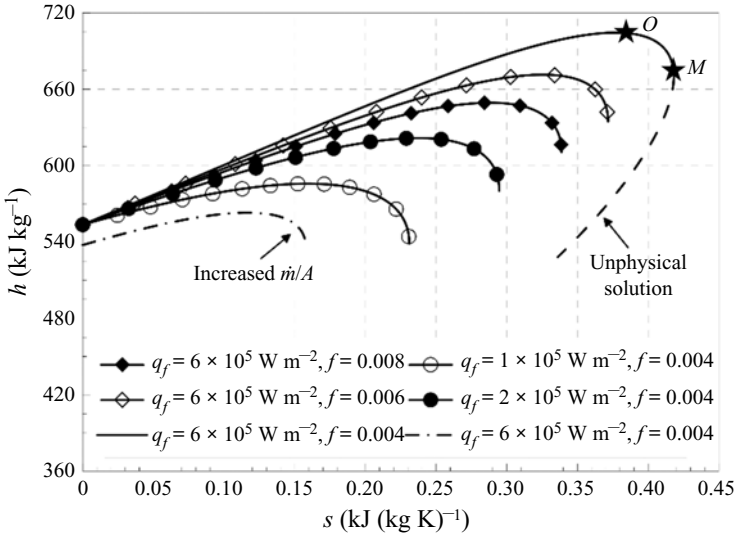

Figure 4. Entropy–enthalpy curves for an initially subsonic flow. The conditions for the tests in the legend: $D = 0.98$ cm, $p_1^0 = 5$ bar, $T_1^0 = 570$ K, $Ma_1 = 0.41$, $\gamma = 1.4$, $R = 287$ J (kg K)$^{-1}$, ($\dot{m} = 41.28$ g s^{-1}).

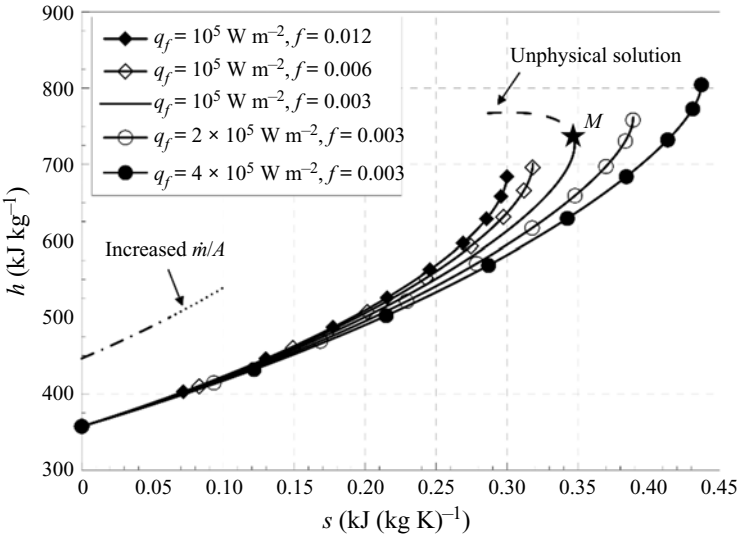

Figure 5. Entropy–enthalpy curves for an initially supersonic flow. The conditions for the tests in the legend: $D = 2.5$ cm, $p_1^0 = 3$ bar, $T_1^0 = 800$ K, $Ma_1 = 2.5$, $\gamma = 1.4$, $R = 287$ J (kg K)$^{-1}$, ($\dot{m} = 79.81$ g s^{-1}).

While the Fanno and Rayleigh h–s curves are unique, once the stagnation point at the pipe inlet and $\dot{m}/A$ have been assigned, infinite h–s curves for the viscous diabatic flow, which depend on the f and $\dot{q}_f$ values, as shown in figures 4 and 5, can exist.

Because a positive heat flux is considered in both figures 4 and 5, s can only increase when the flow goes through the pipe ($\mathrm{d}x > 0$). This is confirmed by the following entropy equation:

$$T\,\mathrm{d}s = \delta q + \delta l_w = \frac{\dot{q}_f \pi D}{\dot{m}}\,\mathrm{d}x + \frac{2f}{D}u^2\,\mathrm{d}x \tag{5.1}$$

Therefore, the increasing entropy gives the direction of the flow evolution along any h–s curve in figures 4 and 5. Any point to the right of an initial point at $s = 0$ along a curve, in either figure 4 or 5, corresponds to the state at the end of a pipe of a certain length L.

For example, the point at $h \approx 700$ kJ kg^{-1} along the continuous-line curve in figure 4 corresponds to the subsonic flow condition at the end of the pipe considered in figure 1 ($L = 50$ cm, $p_V = 2.5$ bar), whereas the point at $h \approx 700$ kJ kg^{-1} along the continuous-line curve in figure 5 corresponds to the supersonic flow condition at the end of the pipe considered in figure 2 ($L = 67.16$ cm, $p_V = 0.56$ bar).

In figure 4, as the flow proceeds along the h–s curve, both the velocity and the Mach number increase, while the pressure decreases. Instead, in figure 5, as the entropy increases, both the velocity and the Mach number reduce, while the pressure increases. These outcomes are in line with those concerning Fanno's flow and Rayleigh's flow for $\dot{q}_f > 0$.

A local maximum point in the entropy can be identified for each curve in both figures 4 and 5 (cf. for example point M). This confirms the presence of a choked flow condition ($Ma_M = 1$) for compressible viscous diabatic flows. If the length of the pipe were increased beyond the L_{chock} value that corresponds to having a critical state like M at the end of the duct, the h–s curves, predicted using the exact solution for $f = 0.004$ and $\dot{q}_f = 6 \times 10^5$ W m^{-2} in figure 4 and for $f = 0.003$ and $\dot{q}_f = 10^5$ W m^{-2} in figure 5, would continue with the dashed lines, but such evolutions would be without any physical meaning because they lead to a reduction in entropy. All this is consistent with the choked flow theory developed for Fanno's flow and for Rayleigh's flow for $\dot{q}_f > 0$ (Shapiro 1953). The unphysical part of the h–s evolution for decreasing entropies has only been reported in one case per figure for explanation (it has been removed for the other curves).

When the final point of the h–s evolution predicted by the exact solution belongs to an unphysical dashed line, it means that the considered problem for the provided boundary conditions does not globally admit any continuous 1-D steady-state solution.

If the flow is initially supersonic and L becomes longer than L_{chock}, the real solution of the compressible viscous diabatic flow will be characterised by the presence of shocks.

Instead, if the flow is initially subsonic and L becomes longer than L_{chock}, no stable solution can be found for the assigned T_1^0, p_1^0, $\dot{m}$, D, f and $\dot{q}_f$ values for the viscous diabatic flow and, after a time transient, the final steady-state solution will feature a lower mass flow rate.

Pipe length L_{chock}, which produces a state like that in M (characterised by a sonic flow) at the final section of the pipe under the assigned T_1^0, p_1^0, $\dot{m}$, D, f and $\dot{q}_f$ values, can be determined for subsonic and supersonic flows by solving the following nonlinear system of algebraic equations, which consists of (3.19), calculated at the final section, x_2, of the pipe, and of relation $Ma_M = 1$ (the unknown variables are u_M, T_M and x_2):

$$\left.\begin{aligned} T_M &= T_1^0 + \frac{\dot{q}_f \pi D}{\dot{m} c_p} x\left(\frac{u_M^2}{2}\right) - \frac{u_M^2}{2c_p} \\ u_M &= \sqrt{\gamma R T_M} \\ x_2 &= L_{chock} = x\left(\frac{u_M^2}{2}\right) \end{aligned}\right\}. \tag{5.2}$$

The maximum entropy of each curve in figures 4 and 5, namely s_M, augments for increasing $\dot{q}_f$ and decreasing f. Because the Rayleigh curve has a higher s_M than the corresponding Fanno curve for fixed γ and the thermodynamic flow state at the pipe inlet,

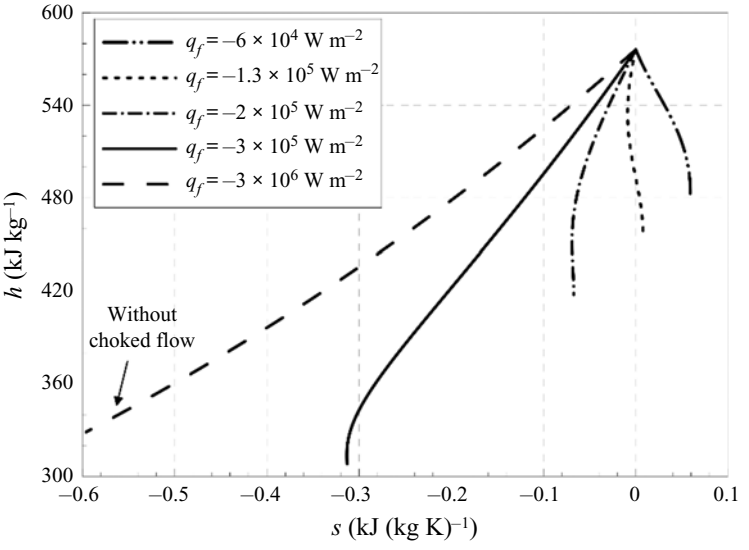

Figure 6. Entropy–enthalpy curves for an initially subsonic flow ($\dot{q}_f < 0$). Test conditions: $D = 0.7$ cm, $p_1^0 = 6$ bar, $T_1^0 = 600$ K, $Ma_1 = 0.48$, $f = 5 \times 10^{-3}$, $\gamma = 1.4$, $R = 287$ J (kg K)$^{-1}$, ($\dot{m} = 27.6$ g s^{-1}).

a larger value of Γ, which is here proportional to the ratio of $\dot{q}_f$ to f ($\dot{m}$, D, p_1^0 and T_1^0 are fixed), leads to a higher value of s_M.

The h–s curves for the subsonic flow in figure 4 also show a local maximum point in the enthalpy (cf. for example point O) and thus in the temperature, in line with Rayleigh's flow.

The abscissa at which the local maximum point in the fluid temperature is reached along the subsonic pipe can be calculated by rewriting (3.3) under the hypothesis $\mathrm{d}T/\mathrm{d}x = 0$, by taking the derivative of function $x(u^2/2)$, as given by (3.18) with respect to $u^2/2$ and, finally, by posing a consistent condition on this derivative with (3.3):

$$\left.\begin{gathered} c_p \frac{\mathrm{d}T}{\mathrm{d}x} + \frac{\mathrm{d}}{\mathrm{d}x}\left(\frac{u^2}{2}\right) = \frac{\mathrm{d}}{\mathrm{d}x}\left(\frac{u^2}{2}\right) = \frac{\dot{q}_f \pi D}{\dot{m}} \\ \frac{\mathrm{d}x}{\mathrm{d}(u^2/2)} = \frac{\dot{m}}{\dot{q}_f \pi D} \end{gathered}\right\}. \tag{5.3}$$

The value of $u^2/2$ at point O can be determined from (5.3). Then, by substituting this value in (3.18), the value of x_O can be determined as a function of f, $\dot{q}_f$ and of the provided boundary conditions of the problem.

No local maximum or minimum points are found for the enthalpy in the supersonic tests in figure 5, irrespective of the values of f and $\dot{q}_f > 0$.

The cases with $\dot{q}_f < 0$ are discussed in the h–s diagrams reported in figures 6 and 7 for subsonic and supersonic flows, respectively. The plotted curves in each graph all start from the same point, that is, at $s = 0$, which corresponds to the initial condition specified in the caption.

The $\dot{q}_f \geq -3 \times 10^5$ W m^{-2} cases in figure 6 all refer to the exact solution reported in (3.18), under the hypothesis that $w^2 + E > 0\,\forall x$, whereas the $\dot{q}_f = -3 \times 10^6$ W m^{-2} case refers to the exact solution reported in (A2) of the appendix (under the hypothesis that $w^2 + E < 0\,\forall x$).

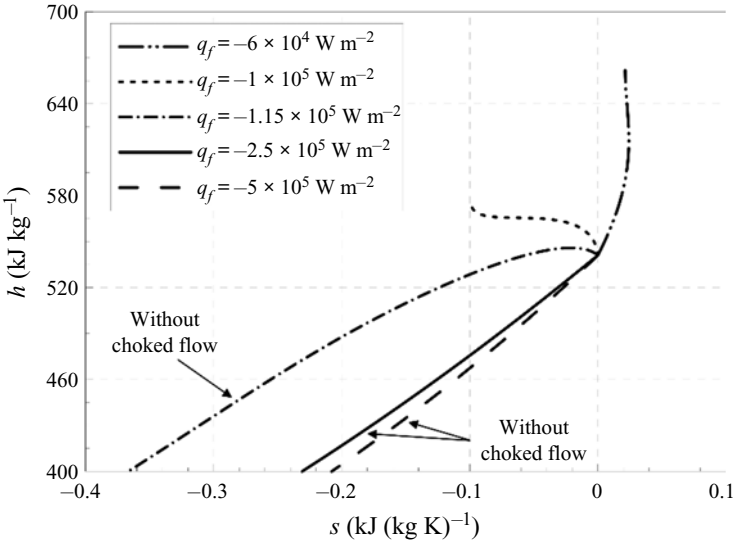

Figure 7. Entropy-enthalpy curves for an initially supersonic flow ($\dot{q}_f < 0$). Test conditions: $D = 3.5$ cm, $p_1^0 = 1.5$ bar, $T_1^0 = 850$ K, $Ma_1 = 1.7, f = 2 \times 10^{-3}$, $\gamma = 1.4$, $R = 287$ J (kg K)$^{-1}$, ($\dot{m} = 149.60$ g s^{-1}).

Furthermore, the $\dot{q}_f \geq -2.5 \times 10^5$ W m^{-2} cases in figure 7 all refer to (3.18), whereas the $\dot{q}_f = -5 \times 10^5$ W m^{-2} case refers to (A2).

In both figures 6 and 7, when $\dot{q}_f < -2f\dot{m}u^2/\pi D^2$, that is, when $\delta q < 0$ prevails over δl_w in (5.1), the entropy locally reduces, whereas the opposite occurs for $\dot{q}_f > -2f\dot{m}u^2/\pi D^2$.

The entropy can also initially reduce and then increase, as is shown in the diagrams referring to the $\dot{q}_f = -1.3 \times 10^5$ W m^{-2} and $\dot{q}_f = -2 \times 10^5$ W m^{-2} cases in figure 6.

When $w^2 + E < 0\,\forall x$, the entropy monotonically reduces (in fact, the negative heat flux in (5.1) clearly prevails over the friction work) along the pipe for both subsonic (cf. figure 6) and supersonic (cf. figure 7) flows, in line with what happens for Rayleigh's flows with a negative heat flux.

A remarkable phenomenon is that choking can be experienced for negative values of $\dot{q}_f$, as shown in both figures 6 and 7 (this does not occur in Rayleigh's flow), even when the negative heat generally prevails over the positive friction work, and most of the evolution, or all the evolution, in the h–s plot occurs for decreasing entropy.

A choked flow is reached along all the curves reported in figure 6, except for $\dot{q}_f = -3 \times 10^6$ W m^{-2}, and it is reached for the $\dot{q}_f = -6 \times 10^4$ W m^{-2} and $\dot{q}_f = -10^5$ W m^{-2} cases in figure 7.

When choking occurs, the h–s curve is interrupted at the choked flow, where $Ma = 1$, and the h–s curve shows a vertical tangent line.

5.2. *Comparisons with the Fanno flow and Rayleigh flow in a dimensionless representation*

According to (3.25) and (3.28), the Mach number versus fx/D_h distribution, pertaining to a compressible viscous diabatic flow, depends on the value of Γ, once Ma_1 and γ have been fixed.

Instead, for the Fanno flow, it is only possible to express Ma as a function of fx/D_h, once Ma_1 and γ have been selected.

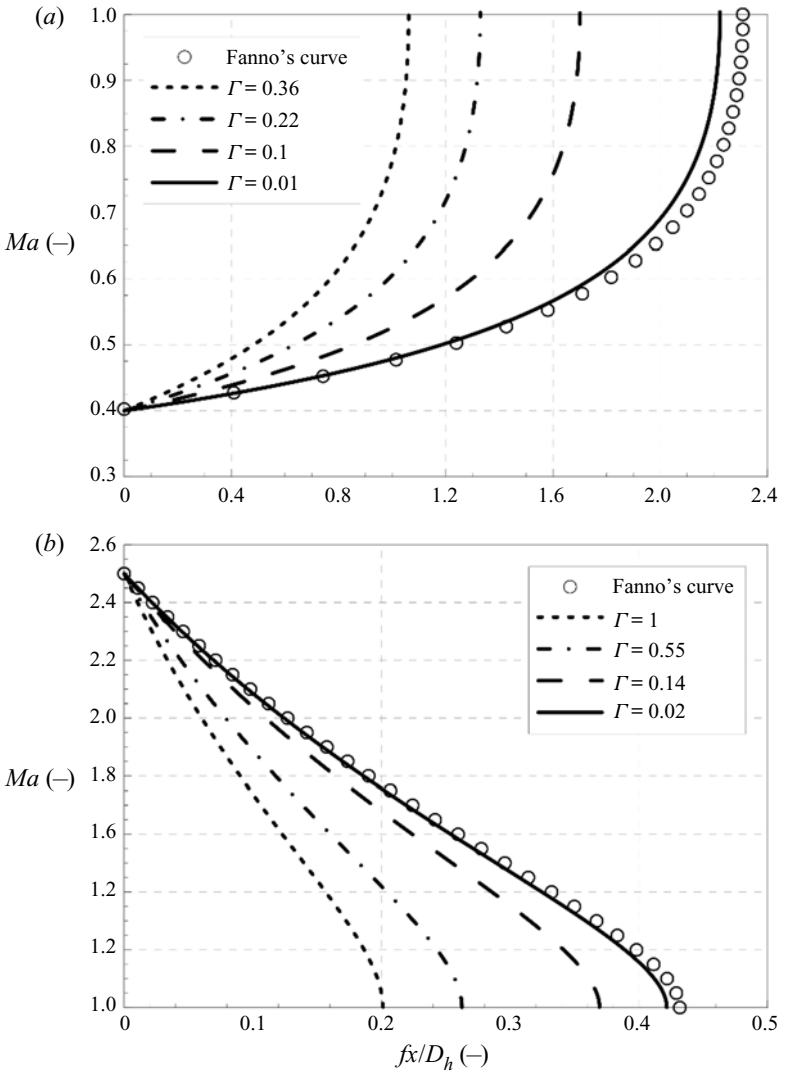

Figure 8. Dimensionless representation in Fanno's mode. (*a*) Subsonic test: $Ma_1 = 0.4$ and (*b*) Supersonic test: $Ma_1 = 2.5$.

Figure 8 compares the Mach versus fx/D_h distributions of the Fanno flow with those referring to compressible viscous diabatic flows for fixed values of Ma_1 and γ.

Figure 8(*a*) is related to a subsonic test, whereas figure 8(*b*) refers to a supersonic test. Different curves, which were obtained by solving (3.25) and (3.28) for different positive values of the Π_L to (fL/D_h) ratio, have been plotted for the compressible viscous diabatic flow.

In general, a lower value of Γ leads to a less important heat transfer effect, compared with the friction effect, and a smaller difference between the Mach versus fx/D_h distributions pertaining to Fanno's and viscous diabatic flows.

When Π_L is sufficiently smaller than (fL/D_h), the compressible viscous diabatic flow distribution virtually coincides with the Fanno flow distribution: this is observed at $\Gamma \approx 0.02$ in the case of the supersonic flow, whereas it still does not occur at $\Gamma \approx 0.01$

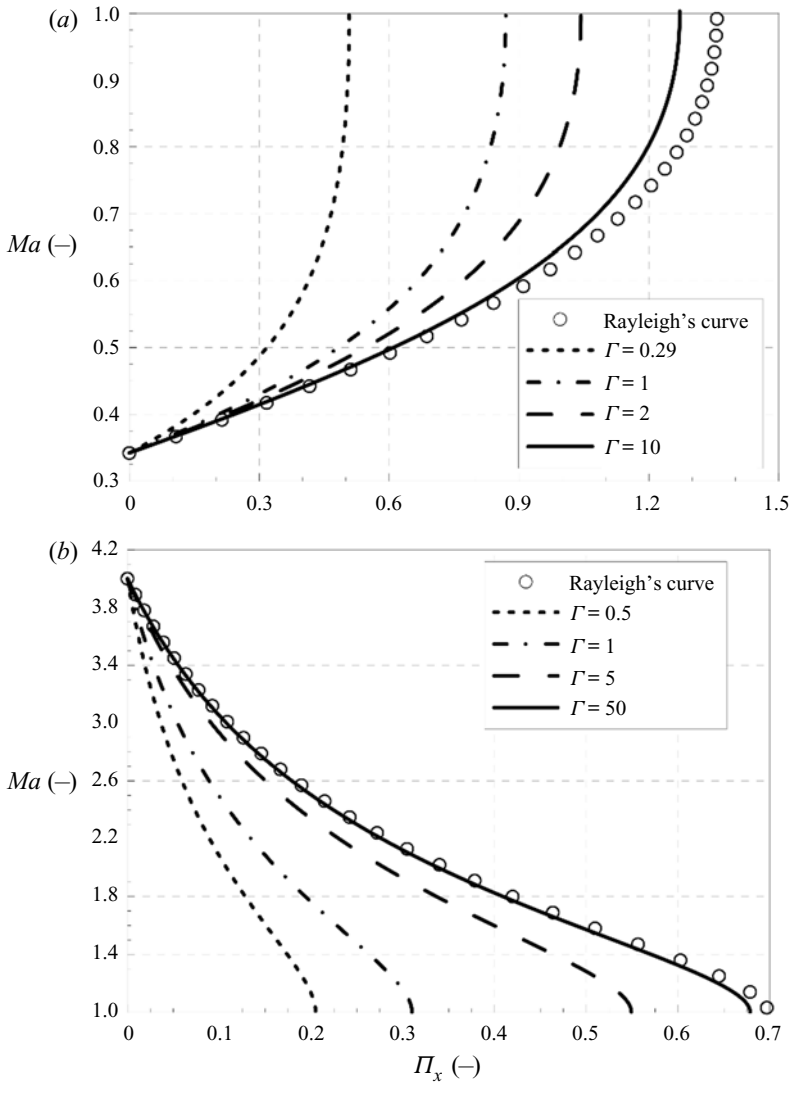

Figure 9. Dimensionless representation in Rayleigh's mode. (*a*) Subsonic test: $Ma_1 = 0.342$ and (*b*) Supersonic test: $Ma_1 = 4$.

in the case of the subsonic flow. There is no general threshold value of Γ below which the Fanno solution can be considered coincident with that of the viscous diabatic flow. In fact, as can be inferred from (3.25) and (3.28), the influence that term Γ can exert on the Ma versus fx/D_h distributions also depends on the value of Ma_1 (γ is fixed in figure 8).

The variation rate of Ma in figure 8 is generally more reduced for the Fanno flow than for viscous diabatic flows.

In the former case, only friction drives the flow changes, whereas, in the latter case, both heat transfer ($\dot{q}_f > 0$) and friction affect Ma in the same way, and this synergy makes Ma grow with fx/D_h at an increased rate.

Therefore, the $Ma = 1$ level is reached at a lower value of fx/D_h when the heat transfer incidence, and thus the value of Γ, augment, as shown in figure 8.

Figure 9 compares the Mach versus Π_x distributions of the compressible viscous diabatic flows obtained from (3.27) and (3.28) with that pertaining to a Rayleigh's flow for fixed values of Ma_1 and γ ($\dot{q}_f$ and thus Π_x take on positive values).

As in the case of figure 8, both subsonic (figure 9*a*) and supersonic (figure 9*b*) tests were performed. The parametric analysis was again made with respect to the value of Γ: a higher value of $\Pi_L/(fL/D_h)$ led to a smaller difference from a Rayleigh's flow. The conclusions are consistent with those shown in figure 8 and when parameter Π_L is sufficiently larger than (fL/D_h), the viscous diabatic flow distribution coincides with the Rayleigh's flow distribution.

Furthermore, the rate of variation of Ma with respect to Π_x, which is generally experienced by the viscous diabatic flow, is larger than that corresponding to a Rayleigh's flow (the $Ma = 1$ level is reached at a lower value of Π_x as Γ decreases).

In short, the analysis presented in figures 8 and 9 proves the physical consistency of (3.25)–(3.28), because the obtained Ma distributions for sufficiently high ($\Gamma \to \infty$) and low ($\Gamma \to 0$) values of Γ match those of the Rayleigh and Fanno models, respectively, which represent the two borderline cases of compressible viscous diabatic flows.

6. Analytical solution for steady-state compressible viscous flows with variable $\dot{q}_f$

The constant heat flux model requires the total heat transfer power with the walls as an input datum of the problem; in fact, as already mentioned in § 3.1, the constant $\dot{q}_f$ is calculated by dividing such a heat power by the inner surface of the pipe. However, $\dot{Q}$ is often an unknown datum of the problem and should be determined *a posteriori* on the basis of the steady-state ODE solution.

Therefore, although the exact solution for the case of constant heat flux represents an important result from the theoretical gas dynamics point of view, it cannot be applied to those engineering problems for which $\dot{Q}$ is not known *a priori*, but represents an outcome of the ODE solution. In fact, the most relevant case for the heat transfer phenomena is that in which $\dot{q}_f$ is expressed as a function of the temperature.

Let us now suppose that the heat flux is variable along the pipe and is expressed according to (2.3). It does not seem possible that an exact solution of the steady-state compressible viscous diabatic flow can be achieved directly in this case, because the resulting ODE of the problem (a second-order ODE with dependent variable h^0 and independent variable x) is markedly nonlinear and cannot be led back to any known typology for which an exact solution exists or can be attempted.

An iterative method is therefore proposed hereafter to determine an approximate analytical solution with the required accuracy. The method is based on the exact solution calculated for the problem with a constant heat flux (cf. § 3): in fact, the pipe is subdivided into different parts of finite length $L_i = x_{i+1} - x_i$ (i is a counter that starts from 1, for which $x_1 = 0$, and arrives at N, for which $x_{N+1} = \sum_i L_i$) and the heat flux is regarded as constant and equal to the space average of effective $\dot{q}_f(x)$ over each part.

Let us preliminarily suppose that the global heat transfer Q (either positive or negative), mass flow rates $\dot{m}$, h_1^0 and $u_1^2/2$ are known data of the problem; this simplifies the illustration of the iterative procedure, but is not a necessary requirement (cf. § 6.1 for further details when Q is unknown). The $w^2 + E > 0\,\forall x$ hypothesis (cf. § 3) is introduced in the following treatment, and the significant mathematical variants, which refer to the $w^2 + E < 0\,\forall x$ case, are given in the appendix.

As a first step of the iterative procedure, an exact solution to the problem with constant $\dot{q}_f$, which is equal to the space-averaged value of $\dot{q}_f(x)$ over L, namely $\bar{\dot{q}}_{f,L} = \dot{Q}/(\pi DL)$,

is calculated according to the approach presented in § 3. This solution represents the first attempt to solve the problem with variable $\dot{q}_f$.

The second step involves the pipe of total length L being divided into N portions (a higher N leads to a more accurate solution), and the following space-averaged value of $\dot{q}_f$ over L_i, i.e. $\bar{\dot{q}}_{f,\,L_i}$, is introduced and defined for each portion as follows:

$$\bar{\dot{q}}_{f,L_i} := \frac{1}{L_i}\int_{x_i}^{x_{i+1}} \lambda(T_w - T)\,\mathrm{d}x = \lambda T_w - \frac{\lambda}{L_i}\int_{x_i}^{x_{i+1}} T\,\mathrm{d}x \quad i = 1, 2, \ldots, N, \tag{6.1}$$

where $\lambda = \lambda(Re,\, Pr)$ can be assumed constant along the pipe. In fact, the Reynolds number and the Prandtl number ($Pr = \mu/c_p\kappa$, where κ is the thermal conductivity of the fluid) can be assumed constant, provided the dependences of c_p, κ and μ on the fluid temperature are neglected (a normally adopted hypothesis for a gas).

The space average of T over L_i, which appears on the right-hand side of (6.1), is estimated using the exact solution pertaining to the $\dot{q}_f = \bar{\dot{q}}_{f,L} = \text{const}$ case for the considered length of pipe.

Hence, rewriting (3.7) for the pipe segment that starts at point x_i, and the length of which is L_i, and dividing this equation by c_p, one obtains

$$T = T_i^0 + \frac{\bar{\dot{q}}_{f,L}\pi D}{\dot{m}c_p}(x - x_i) - \frac{u^2}{2c_p} \quad i = 1, 2, \ldots, N, \tag{6.2}$$

where $T_i^0 = h_i^0/c_p$ is the value of the total temperature at x_i. Such a value is calculated directly from the boundary datum h_1^0 for $i = 1$ ($x_1 = 0$) and it can be calculated from (3.18) and (3.19), with $\dot{q}_f = \bar{\dot{q}}_{f,\,L} = \text{const}$, for all the other i values.

By substituting the expression of T, given by (6.2), in the integral in (6.1), the following formula can be obtained for a first attempt at evaluating $\bar{\dot{q}}_{f,\,L_i}$:

$$\bar{\dot{q}}^{(1)}_{f,L_i} \approx \lambda[T_w - T^0(x_i)] - \frac{\lambda\bar{\dot{q}}_{f,L}\pi D L_i}{2\dot{m}c_p} + \frac{\lambda}{L_i c_p}\int_{x_i}^{x_{i+1}} \frac{u^2}{2}\,\mathrm{d}x \quad i = 1, 2, \ldots, N. \tag{6.3}$$

On the basis of (3.10), and taking both (3.9) and its differentiation $\mathrm{d}t = 2/u^2\,\mathrm{d}(u^2/2)$ into account, one obtains ($y := u^2/2$ for conciseness of notation)

$$\int_{x_i}^{x_{i+1}} y\,\mathrm{d}x = \int_{y_i}^{y_{i+1}} \left(\frac{\dfrac{\gamma-1}{2\gamma}\dfrac{\bar{\dot{q}}_{f,L}\pi D}{\dot{m}}}{\dfrac{4f}{D}y + \dfrac{\gamma-1}{\gamma}\dfrac{\bar{\dot{q}}_{f,L}\pi D}{\dot{m}}} \right) x(y)\,\mathrm{d}y + \int_{y_i}^{y_{i+1}} \left(\frac{\dfrac{\gamma-1}{2\gamma}h_i^0 - \dfrac{\gamma+1}{2\gamma}y}{\dfrac{4f}{D}y + \dfrac{\gamma-1}{\gamma}\dfrac{\bar{\dot{q}}_{f,L}\pi D}{\dot{m}}} \right) \mathrm{d}y. \tag{6.4}$$

The left-hand side member of this equation is the same as the space integral in (6.3). The two space integrals on the right-hand side of (6.4) can be further decomposed into other integrals that can then be solved analytically (Dwight 1961), according to what is reported in table 1. As a result, it is possible to determine an analytical expression for $\bar{\dot{q}}^{(1)}_{f,L_i}(i = 1, 2, \ldots, N)$ by substituting the analytical expression of $\int_{x_i}^{x_{i+1}} u^2/2\,\mathrm{d}x$, which is reported as the final result in table 1 (cf. step IV), in (6.3).

The third step of the procedure consists in calculating a new analytical solution, which refers to the $\dot{q}_f = \bar{\dot{q}}^{(1)}_{f,L_i} = \text{const}$ case, for each piece of pipe that extends from x_i to x_{i+1}.

https://doi.org/10.1017/jfm.2021.278 Published online by Cambridge University Press

I) Definitions: $J_i := \dfrac{\dot{m}h_i^0}{\bar{\dot{q}}_{f,L}\pi D}, \quad K := \dfrac{\gamma+1}{\gamma}\dfrac{D}{4f}, \quad S := \dfrac{\gamma-1}{\gamma}\dfrac{\bar{\dot{q}}_{f,L}\pi D^2}{4f\dot{m}},$

$U_i := \dfrac{\gamma-1}{2\gamma}h_i^0, \quad V := \dfrac{\gamma+1}{2\gamma}, \quad W := \dfrac{4f}{D}, \quad Z := \dfrac{\gamma-1}{\gamma}\dfrac{\bar{\dot{q}}_{f,L}\pi D}{\dot{m}}$

II) $\displaystyle\int_{y_i}^{y_{i+1}} \frac{U_i - Vy}{Wy+Z}\,\mathrm{d}y = \int_{y_i}^{y_{i+1}} \frac{U_i}{Wy+Z}\,\mathrm{d}y - \int_{y_i}^{y_{i+1}} \frac{Vy}{Wy+Z}\,\mathrm{d}y$

$\displaystyle\int_{y_i}^{y_{i+1}} \frac{U_i}{Wy+Z}\,\mathrm{d}y = \frac{U_i}{W}\ln(Wy+Z)\Big|_{y_i}^{y_{i+1}}, \quad \int_{y_i}^{y_{i+1}} \frac{Vy}{Wy+Z}\,\mathrm{d}y = \frac{V}{W}y\Big|_{y_i}^{y_{i+1}} - \frac{VZ}{W^2}\ln(Wy+Z)\Big|_{y_i}^{y_{i+1}}$

III) $\displaystyle x(y) = x_i - J_i + \left\{C_i - K\ln\left[\frac{\sqrt{y}+\sqrt{y+S}}{\sqrt{|S|}}\right]\right\}\frac{\sqrt{y}}{\sqrt{y+S}} \quad \text{with } C_i = J_i\frac{\sqrt{y_i+S}}{\sqrt{y_i}} + K\ln\left[\frac{\sqrt{y_i}+\sqrt{y_i+S}}{\sqrt{|S|}}\right]$

$\displaystyle\int_{y_i}^{y_{i+1}} \frac{S/2}{y+S}x(y)\,\mathrm{d}y = \int_{y_i}^{y_{i+1}} \left[\frac{x_iS - J_iS}{2(y+S)} + \frac{C_iS\sqrt{y}}{2(y+S)^{3/2}} - \frac{KS\sqrt{y}}{2(y+S)^{3/2}}\ln\left(\frac{\sqrt{y}+\sqrt{y+S}}{\sqrt{|S|}}\right)\right]\mathrm{d}y$

$\displaystyle\int_{y_i}^{y_{i+1}} \left[-\frac{J_iS}{2(y+S)}\right]\mathrm{d}y = -\frac{J_iS}{2}\ln(y+S)\Big|_{y_i}^{y_{i+1}}, \quad \int_{y_i}^{y_{i+1}} \left[\frac{C_iS\sqrt{y}}{2(y+S)^{3/2}}\right]\mathrm{d}y = C_iS\left[\ln(\sqrt{y}+\sqrt{y+S}) - \frac{\sqrt{y}}{\sqrt{y+S}}\right]\Big|_{y_i}^{y_{i+1}}$

$\displaystyle\int_{y_i}^{y_{i+1}} \left[-\frac{KS\sqrt{y}}{2(y+S)^{3/2}}\ln\left(\frac{\sqrt{y}+\sqrt{y+S}}{\sqrt{|S|}}\right)\right]\mathrm{d}y = \int_{y_i}^{y_{i+1}} \left[\frac{KS\sqrt{y}}{2(y+S)^{3/2}}\ln\left(\sqrt{|S|}\right)\right]\mathrm{d}y - \int_{y_i}^{y_{i+1}} \left[\frac{KS\sqrt{y}}{2(y+S)^{3/2}}\ln\left(\sqrt{y}+\sqrt{y+S}\right)\right]\mathrm{d}y$

$\displaystyle\int_{y_i}^{y_{i+1}} \left[\frac{KS\sqrt{y}}{2(y+S)^{3/2}}\ln\left(\sqrt{|S|}\right)\right]\mathrm{d}y = KS\ln\left(\sqrt{|S|}\right)\left[\ln(\sqrt{y}+\sqrt{y+S}) - \frac{\sqrt{y}}{\sqrt{y+S}}\right]\Big|_{y_i}^{y_{i+1}}$

$\displaystyle\int_{y_i}^{y_{i+1}} \left[\frac{KS\sqrt{y}}{2(y+S)^{3/2}}\ln(\sqrt{y}+\sqrt{y+S})\right]\mathrm{d}y = \frac{KS}{2}\left[\ln^2(\sqrt{y}+\sqrt{y+S}) - \frac{2\sqrt{y}}{\sqrt{y+S}}\ln(\sqrt{y}+\sqrt{y+S}) + \ln(y+S)\right]\Big|_{y_i}^{y_{i+1}}$

IV) $\displaystyle\int_{x_i}^{x_{i+1}} y\,\mathrm{d}x = \frac{U_i}{W}\ln(Wy+Z)\Big|_{y_i}^{y_{i+1}} + \frac{VZ}{W^2}\ln(Wy+Z)\Big|_{y_i}^{y_{i+1}} + \left[C_iS + KS\ln\left(\sqrt{|S|}\right)\right]\cdot\left[\ln\left(\sqrt{y}+\sqrt{y+S}\right) - \frac{\sqrt{y}}{\sqrt{y+S}}\right]\Big|_{y_i}^{y_{i+1}}$

$\displaystyle + \frac{(x_iS - J_iS)}{2}\ln(y+S)\Big|_{y_i}^{y_{i+1}} - \frac{V}{W}y\Big|_{y_i}^{y_{i+1}} - \frac{KS}{2}\left[\ln^2\left(\sqrt{y}+\sqrt{y+S}\right) - \frac{2\sqrt{y}}{\sqrt{y+S}}\ln\left(\sqrt{y}+\sqrt{y+S}\right) + \ln(y+S)\right]\Big|_{y_i}^{y_{i+1}}$

Table 1. Analytical calculus steps of the $\int y\,\mathrm{d}x$ integral in (6.4).

On the basis of (3.18) and (3.21), the following $x = x(u^2/2)$ distribution can be achieved $(x_i \le x \le x_{i+1})$:

$$x - x_i = -\frac{\dot{m}h_i^0}{\bar{\dot{q}}_{f,L_i}^{(1)}\pi D} + \left\{ C_i - \frac{\gamma+1}{\gamma}\frac{D}{4f}\ln\left[\frac{\sqrt{\frac{u^2}{2}} + \sqrt{\frac{u^2}{2} + \frac{\gamma-1}{\gamma}\frac{\bar{\dot{q}}_{f,L_i}^{(1)}\pi D^2}{4f\dot{m}}}}{\sqrt{\frac{\gamma-1}{\gamma}\frac{|\bar{\dot{q}}_{f,L_i}^{(1)}|\pi D^2}{4f\dot{m}}}}\right]\right\} \times \frac{\sqrt{\frac{u^2}{2}}}{\sqrt{\frac{u^2}{2} + \frac{\gamma-1}{\gamma}\frac{\bar{\dot{q}}_{f,L_i}^{(1)}\pi D^2}{4f\dot{m}}}} \quad i = 1, 2, .., N, \tag{6.5}$$

where C_i is given by

$$C_i = \frac{\dot{m}h_i^0}{\bar{\dot{q}}_{f,L_i}^{(1)}\pi D}\frac{\sqrt{\frac{u_i^2}{2} + \frac{\gamma-1}{\gamma}\frac{\bar{\dot{q}}_{f,L_i}^{(1)}\pi D^2}{4f\dot{m}}}}{\sqrt{\frac{u_i^2}{2}}} + \frac{\gamma+1}{\gamma}\frac{D}{4f}\ln\left[\frac{\sqrt{\frac{u_i^2}{2}} + \sqrt{\frac{u_i^2}{2} + \frac{\gamma-1}{\gamma}\frac{\bar{\dot{q}}_{f,L_i}^{(1)}\pi D^2}{4f\dot{m}}}}{\sqrt{\frac{\gamma-1}{\gamma}\frac{|\bar{\dot{q}}_{f,L_i}^{(1)}|\pi D^2}{4f\dot{m}}}}\right]. \tag{6.6}$$

The second and third steps of the described procedure should be repeated replacing $\bar{\dot{q}}_{f,L}$ with $\bar{\dot{q}}_{f,L_i}^{(1)}$ in (6.2)–(6.4) as well as in table 1: a second-attempt approximation of $\bar{\dot{q}}_{f,L_i}$, namely $\bar{\dot{q}}_{f,L_i}^{(2)}$, can be determined from (6.3) and it can be used to obtain a new solution from (6.5) (that is, $\bar{\dot{q}}_{f,L_i}^{(2)}$ replaces $\bar{\dot{q}}_{f,L_i}^{(1)}$ in (6.3) and (6.5)). When the iteration process arrives at the final round, (6.5) gives the correct distribution $x = x(u^2/2)$ along each L_i ($i = 1,2\ldots,N$), (6.2) and (6.5) provide the corresponding $T(x)$ distribution, and (2.3), (6.2) and (6.5) provide the final $\dot{q}_f(x)$ distribution.

In short, the presented analytical solution to the compressible viscous diabatic flow with variable $\dot{q}_f$ given by (2.3) is a piecewise approximate solution. Each of the N analytical pieces coincides with the exact solution of a problem that refers to a constant heat flux, which is virtually equal to the exact value of the average $\dot{q}_f(x)$ over L_i, namely $\bar{\dot{q}}_{f,L_i}(i = 1, 2, \ldots, N)$. As soon as N is increased by one, and the patterns of the piecewise analytical solution do not change appreciably, compared with those pertaining to the preceding N value, a piecewise analytical solution is reached that is almost equivalent to the exact solution of the problem.

6.1. *Validation of the developed solution*

Figures 10 and 11 plot the validation tests for the steady-state analytical solutions of viscous diabatic flows with a positive variable heat flux in the cases of subsonic and supersonic motion, respectively. In both cases, the analytical solution was determined by applying (6.1)–(6.6) iteratively, together with the relations reported in table 1.

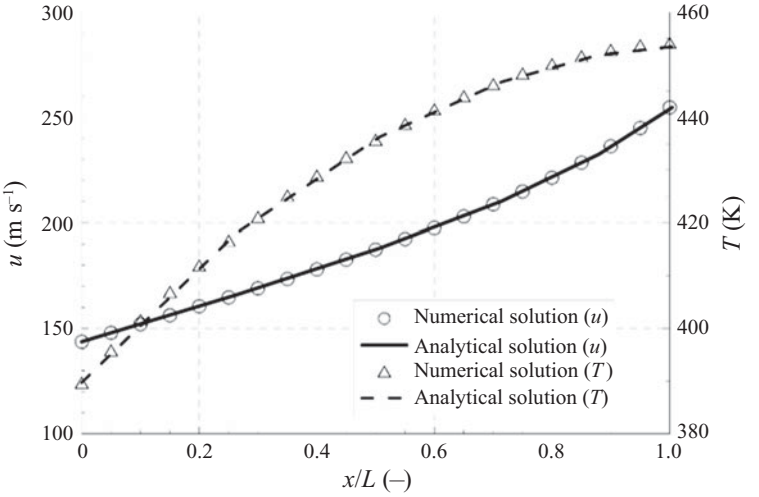

Figure 10. Validation test for the analytical solution with a variable heat flux for a subsonic flow. Test conditions: $L = 200$ cm, $D = 1.96$ cm, $p_1^0 = 1$ bar, $T_1^0 = 400$ K, $p_V = 0.6$ bar, $f = 4 \times 10^{-3}$, $\lambda = 364$ W (m^2 K)$^{-1}$, $T_w = 500$ K, $\gamma = 1.4$, $R = 287$ J (kg K)$^{-1}$, $N = 5$, $\Delta x = 1$ mm ($\dot{m} = 35.47$ g s^{-1}).

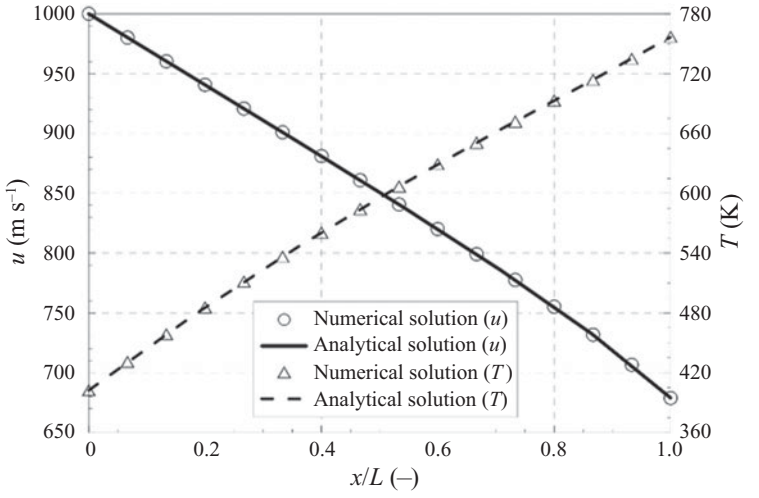

Figure 11. Validation test for the analytical solution with a variable heat flux for a supersonic flow. Test conditions: $L = 45$ cm, $D = 1.96$ cm, $p_1^0 = 2.51$ bar, $T_1^0 = 900$ K, $Ma_1 = 2.49$, $f = 3 \times 10^{-3}$, $\lambda = 423$ W (m^2 K)$^{-1}$, $T_w = 880$ K, $\gamma = 1.4$, $R = 287$ J (kg K)$^{-1}$, $N = 6$, $\Delta x = 0.1$ mm ($\dot{m} = 39.28$ g s^{-1}).

Finally, the convective heat transfer power with the walls was evaluated using the formula

$$\dot{Q} \approx \pi D \sum_{i=1}^{N} \bar{\dot{q}}_{f,\,L_i}^{(J+1)} L_i, \tag{6.7}$$

where the value J corresponds to the final iteration for the velocity distribution and $\bar{\dot{q}}_{f,L_i}^{(J+1)}$ comes from (6.3) after approximating $\bar{\dot{q}}_{f,L_i}$ with $\bar{\dot{q}}_{f,\,L_i}^{(J)}$, and introducing the velocity and temperature distributions obtained at the end of iteration J.

The PDE numerical solution used for validation in figures 10 and 11 was obtained as described in § 4. It is based on the discretisation of (2.1), (2.2) and (2.4), and $\dot{q}_f$ is expressed using (2.3).

As can be observed, the agreement between the numerical and analytical solutions in figures 10 and 11 is satisfactory (the percentage differences between these solutions are lower than 1 %) and the corresponding predictions of the total heat transfer are virtually the same (the differences between the numerical and analytical $\dot{Q}$ predictions result to be lower than or equal to 1 %). The accuracy obtained for the $\dot{Q}$ prediction via (6.7) is important because it proves that each $\bar{\dot{q}}_{f,L_i}^{(J+1)}$ $(i = 1, 2, \ldots, N)$ is virtually coincident with the space average of the effective $\dot{q}_f(x)$ over L_i. This further confirms the physical consistency of the procedure.

The pipe was subdivided into $N = 5$ and $N = 6$ pieces for the validation tests shown in figures 10 and 11, respectively. In both cases, convergence to the exact solution was reached for each piece L_i of the pipe after few iterations.

The initial value of $\bar{\dot{q}}_{f,L}$ used in the first-attempt solution with a constant heat flux over the pipe (cf. § 6) could not be equal to $\dot{Q}/(\pi DL)$, because $\dot{Q}$ was unknown in the tests: therefore, $\bar{\dot{q}}_{f,L} \approx \lambda(T_w - T_1)$ was assumed in the first step of the iterative procedure.

Furthermore, the mass flow rate of the supersonic flow in figure 11 was calculated easily using (3.20), because the T_1^0, p_1^0 and Ma_1 boundary conditions were assigned at the pipe inlet.

Instead, the mass flow rate for the subsonic test in figure 10 was evaluated with the shooting iterative procedure explained in § 3.1, because p_V was assigned in addition to T_1^0 and p_1^0. Hence, a tentative value of Ma_1 was used for the subsonic flow to evaluate tentative $u_1^2/2$ and T_1 values at the pipe inlet as well as a tentative mass flow rate $\dot{m}$ through the whole pipe (the value of $\dot{m}$ is shared between the N lengths of the pipe). The pressure value, p_2, at the end section of the whole pipe ($x_2 = L$), predicted using the piecewise analytical solution after the iterations on $\bar{\dot{q}}_{f,L_i}\,\forall i$, was then compared with the p_V value, and a final cycle of iterations was performed on Ma_1 until the difference between p_2 and p_V was within a prescribed tolerance. When the mass flow rate is provided as an input datum to the steady-state subsonic problem (in addition to p_1^0 and T_1^0), the iterations on Ma_1 are not performed and the whole procedure is simplified.

It is worth pointing out that the difficulty in determining the unknown flow-rate is not a drawback of the proposed analytical solutions for compressible viscous diabatic flows, and is also typical of the Fanno and Rayleigh models, which require iterative procedures for the calculus of $\dot{m}$ when p_V, T_1^0 and p_1^0 are the input data to the problem.

Analogous tests to those presented in figures 10 and 11 have been carried out successfully with a negative variable heat flux under the $w^2 + E > 0\,\forall x$ condition, but they have not been reported here for the sake of conciseness.

7. Conclusions

New analytical solutions have been obtained for the 1-D steady-state compressible viscous diabatic flow of an ideal gas through a constant cross-section pipe. Such solutions are valid for both subsonic and supersonic flows and extend the set of gas dynamics analytical solutions.

As a first result, an exact solution was obtained for the case of either a positive or negative constant heat flux with the walls.

The original set of nonlinear Euler generalised ODEs for the steady-state 1-D flow was reduced to a single, linear, first-order ODE with variable coefficients. To obtain a linear ODE that can be solved analytically, it is essential to determine the right transformations of the variables and to identify the kinetic energy per unit of mass as the physical variable that should appear in the final ODE of the problem.

Moreover, as a second result, the obtained exact solution has been represented in dimensionless form by reducing the number of parameters and variables with respect to the dimensional ODE.

Two dimensionless representations have been proposed: in the Fanno mode representation, the Mach number can be plotted as a function of the fx/D_h group, whereas, in the Rayleigh mode representation, the Mach number can be plotted as a function of the dimensionless group $\Pi_x = \dot{q}_f \pi D x/\dot{m} h_1^0$. In both cases, different curves can be obtained on a graph for different values of the Γ parameter, which is defined by the ratio of Π_L to (fL/D_h). When Γ is sufficiently large ($\Gamma \to \infty$), the developed analytical solution for the compressible viscous diabatic flow tends to Rayleigh's model, whereas, when Γ is sufficiently small ($\Gamma \to 0$), it tends to Fanno's model.

As a third result, an iterative method has been developed to determine an approximate analytical solution for the case of the 1-D viscous compressible flow along a constant cross-section pipe in the presence of a variable convective heat flux with the walls. This is a more relevant and general case for engineering applications than that with $\dot{q}_f = \text{const}$, because it is not necessary to know the total heat transfer power exchanged with the walls *a priori* to calculate the solution.

Because the problem with variable $\dot{q}_f$ is affected by strong nonlinearity, it is not possible to find a direct exact solution for this case. The duct was subdivided into N lengths L_i ($i = 1,2,\ldots,N$) and the heat flux with the walls was assumed constant in each portion: the exact solution to the $\bar{\dot{q}}_{f,L_i} = \text{const}$ problem was therefore applied to each piece of the pipe. After a few iterations, the value of the constant heat flux in each piece converges to the space average of the effective heat flux $\dot{q}_f(x)$ over length L_i. The developed iterative methodology converges rapidly to an analytical solution and the accuracy of this solution can be improved by increasing the value of N.

As a fourth result, the developed exact and approximate analytical solutions for constant (both positive and negative) and variable $\dot{q}_f$ have been validated successfully through a comparison with the corresponding numerical time asymptotic solutions of the generalised Euler equations.

Finally, the compressible viscous diabatic flows have been discussed in enthalpy–entropy diagrams, on the basis of the curves obtained from the exact solutions for the $\dot{q}_f = \text{const}$ case. Although the Fanno and Rayleigh curves in an h–s diagram are unique, once the stagnation point at the pipe inlet (T_1^0, p_1^0) and the value of $\dot{m}/A$ have been assigned, the corresponding h–s curves for the viscous diabatic flows are infinite, and depend on the f and $\dot{q}_f$ values (the synthetic dependence is on $\dot{q}_f/f$). Choking can occur for both the $\dot{q}_f > 0$ and $\dot{q}_f < 0$ conditions for compressible viscous diabatic flows. In the case of a negative heat flux, choking can also be observed when the negative heat prevails over the positive friction work and most of the evolution or all the evolution occurs with decreasing entropy.

Declaration of interests. The author reports no conflict of interest.

Author ORCIDs.
Alessandro Ferrari http://orcid.org/0000-0001-6980-2325.

Appendix

When condition $w^2 + E < 0\,\forall x$ holds (cf. § 3 for the expressions of w and E), the integrals in (3.17) are replaced by the following integrals

$$\left.\begin{aligned}\int \frac{G}{\sqrt{-w^2-E}}\,\mathrm{d}w &= G\arcsin\left(\frac{w}{\sqrt{|E|}}\right)\\ \int \frac{F}{w^2\sqrt{-w^2-E}}\,\mathrm{d}w &= \frac{F}{E}\frac{\sqrt{-w^2-E}}{w}\end{aligned}\right\}, \tag{A1}$$

and the analytical solution given in (3.18) is modified as follows ($\dot{q}_f$ must be negative in this case):

$$x = \frac{\dot{m}h_1^0}{|\dot{q}_f|\pi D} + \left\{C + \frac{\gamma+1}{\gamma}\frac{D}{4f}\arcsin\left[\frac{\sqrt{\dfrac{u^2}{2}}}{\sqrt{\dfrac{\gamma-1}{\gamma}\dfrac{|\dot{q}_f|\pi D^2}{4f\dot{m}}}}\right]\right\}\frac{\sqrt{\dfrac{u^2}{2}}}{\sqrt{\dfrac{\gamma-1}{\gamma}\dfrac{|\dot{q}_f|\pi D^2}{4f\dot{m}} - \dfrac{u^2}{2}}}. \tag{A2}$$

The constant C can be calculated by solving (A2) under the condition $u^2/2 = u_1^2/2$ at $x = x_1 = 0$:

$$C = -\frac{\dot{m}h_1^0}{|\dot{q}_f|\pi D}\frac{\sqrt{\dfrac{\gamma-1}{\gamma}\dfrac{|\dot{q}_f|\pi D^2}{4f\dot{m}} - \dfrac{u_1^2}{2}}}{\sqrt{\dfrac{u_1^2}{2}}} - \frac{\gamma+1}{\gamma}\frac{D}{4f}\arcsin\left[\frac{\sqrt{\dfrac{u_1^2}{2}}}{\sqrt{\dfrac{\gamma-1}{\gamma}\dfrac{|\dot{q}_f|\pi D^2}{4f\dot{m}}}}\right]. \tag{A3}$$

Equation (A3) replaces (3.21). Equations (A2) and (A3) provide the exact solution under the hypothesis $w^2 + E < 0\,\forall x$. This new solution has been validated successfully in figure 12, where a comparison has been performed with the results of a numerical simulation for the case of a supersonic flow.

Unlike figure 2, which refers to the $w^2 + E > 0\,\forall x$ case, the velocity increases and the temperature reduces along the supersonic pipe. These trends of u and T, with respect to x, in figure 12 are of the same type as those experienced in Rayleigh's supersonic flows with a negative heat flux.

The procedure used to obtain a dimensionless representation for (A2) is similar to that described for (3.18) in § 3.2. The outcome is analogous: either the Mach number or the Crocco number can be expressed as functions of either fx/D_h or Π_x, according to Fanno's or Rayleigh's mode representations, respectively, and Γ is a parameter of the solution (the other parameters are Ma_1 and γ).

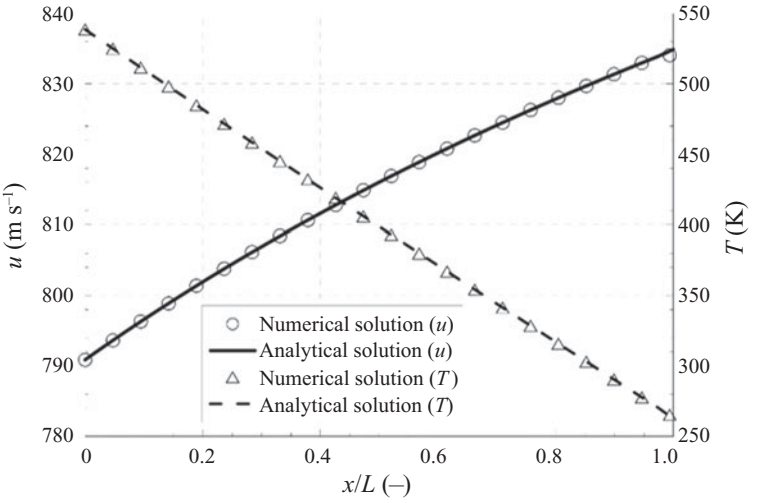

Figure 12. Validation test for the analytical solution under the hypothesis of $w^2 + E < 0\,\forall x$ for a supersonic flow. Test conditions: $L = 65.5$ cm, $D = 3.5$ cm, $p_1^0 = 1.5$ bar, $T_1^0 = 850$ K, $Ma_1 = 1.7$, $f = 2 \times 10^{-3}$, $\dot{q}_f = -5 \times 10^5$ W m^{-2}, $\gamma = 1.4$, $R = 287$ J (kg K)$^{-1}$, $\Delta x = 1$ mm ($\dot{m} = 14.96$ g s^{-1}).

Finally, let us suppose that $w^2 + E = 0$ at a certain x value. Without losing any generality, we can assume that this happens at point $x_1 = 0$ (the following condition leads to a decrease in entropy):

$$\frac{u_1^2}{2} + \frac{\gamma - 1}{\gamma}\frac{\dot{q}_f \pi D^2}{4 f \dot{m}} = 0 \Rightarrow \dot{q}_f = -\frac{2\gamma}{\gamma - 1}\frac{f \dot{m} u_1^2}{\pi D^2}. \tag{A4}$$

Neither (3.18) nor (A2) can be used because the denominators in the expressions go to zero. By taking (A4) and (3.7) into account, (3.8) simplifies to

$$\left(h^0 - \frac{\gamma + 1}{\gamma - 1}\frac{u^2}{2}\right)\frac{\mathrm{d}}{\mathrm{d}x}\left(\frac{u^2}{2}\right) = 0. \tag{A5}$$

If $u^2 \neq 2c_p T^0(\gamma - 1)/(\gamma + 1)$ (the equality corresponds to a choked flow with $Ma = 1$), a general solution to (A5) is given by $u = \text{const}$. This means that, for (3.1), the thermodynamic evolution is isochoric ($\rho = \text{const}$). The temperature distribution can easily be calculated from (3.7):

$$T(x) = T_1^0 + \frac{\dot{q}_f \pi D}{\dot{m} c_p} x - \frac{u_1^2}{2c_p}, \tag{A6}$$

where the value of $\dot{q}_f$ is obviously given by (A4). As can be inferred, the temperature decreases linearly with x and the same occurs for the pressure, which can be calculated from (3.4).

As far as the iterative solution to the case of the variable $\dot{q}_f$ is concerned, the methodology described in § 6 remains the same when the exact solution for the $\dot{q}_f = \text{const}$ case is given by (A2) and (A3). Obviously, (6.5) should be substituted with a corresponding expression, based on (A2), and the solution to (6.4) involves different integrals from those indicated in table 1.

The integrals corresponding to those in table 1 are reported in table 2 for the $w^2 + E < 0$ case. The essential point is that all the integrals in table 2 can be solved analytically.

https://doi.org/10.1017/jfm.2021.278 Published online by Cambridge University Press

I) Definitions as in Table 1

II) $$\int_{y_i}^{y_{i+1}} \frac{U_i - Vy}{Wy - |Z|}\,\mathrm{d}y = \frac{U_i}{W}\ln\left(|Z| - Wy\right)\Big|_{y_i}^{y_{i+1}} - \frac{V}{W}y\Big|_{y_i}^{y_{i+1}} - \frac{V|Z|}{W^2}\ln(|Z| - Wy)\Big|_{y_i}^{y_{i+1}}$$

III) $$x(y) = x_i + |J_i| + \left\{C_i + K\arcsin\left(\frac{\sqrt{y}}{\sqrt{|S|}}\right)\right\}\frac{\sqrt{y}}{\sqrt{|S|-y}} \quad \text{with } C_i = -|J_i|\frac{\sqrt{|S|-y_i}}{\sqrt{y_i}} - K\arcsin\left(\frac{\sqrt{y_i}}{\sqrt{|S|}}\right)$$

$$\int_{y_i}^{y_{i+1}} \frac{S/2}{y-|S|}x(y)\,\mathrm{d}y = \int_{y_i}^{y_{i+1}}\left[\frac{-(x_i+|J_i|)S}{2(|S|-y)} - \frac{C_iS\sqrt{y}}{2(|S|-y)^{3/2}} - \frac{KS\sqrt{y}}{2(|S|-y)^{3/2}}\arcsin\left(\frac{\sqrt{y}}{\sqrt{|S|}}\right)\right]\mathrm{d}y$$

$$\int_{y_i}^{y_{i+1}}\left[\frac{-|J_i|S}{2(|S|-y)}\right]\mathrm{d}y = \frac{|J_i|S}{2}\ln(|S|-y)\Big|_{y_i}^{y_{i+1}}, \quad \int_{y_i}^{y_{i+1}}\left[\frac{-C_iS\sqrt{y}}{2(|S|-y)^{3/2}}\right]\mathrm{d}y = C_iS\left[\arcsin\left(\frac{\sqrt{y}}{\sqrt{|S|}}\right) - \frac{\sqrt{y}}{\sqrt{|S|-y}}\right]\Big|_{y_i}^{y_{i+1}}$$

$$\int_{y_i}^{y_{i+1}}\left[-\frac{KS\sqrt{y}}{2(|S|-y)^{3/2}}\arcsin\left(\frac{\sqrt{y}}{\sqrt{|S|}}\right)\right]\mathrm{d}y = KS\left\{\left[\arcsin\left(\frac{\sqrt{y}}{\sqrt{|S|}}\right) - \frac{\sqrt{y}}{\sqrt{|S|-y}}\right]\cdot\arcsin\left(\frac{\sqrt{y}}{\sqrt{|S|}}\right)\right\}\Big|_{y_i}^{y_{i+1}}$$
$$-\frac{KS}{2}\left[\arcsin\left(\frac{\sqrt{y}}{\sqrt{|S|}}\right)\right]^2\Big|_{y_i}^{y_{i+1}} - \frac{KS}{2}\ln(|S|-y)\Big|_{y_i}^{y_{i+1}}$$

IV) $$\int_{x_i}^{x_{i+1}} y\,\mathrm{d}x = \left[\frac{U_iW - V|Z|}{W^2}\ln\left(|Z| - Wy\right) - \frac{V}{W}y\right]\Big|_{y_i}^{y_{i+1}} + C_iS\left[\arcsin\left(\frac{\sqrt{y}}{\sqrt{|S|}}\right) - \frac{\sqrt{y}}{\sqrt{|S|-y}}\right]\Big|_{y_i}^{y_{i+1}}$$
$$+\frac{x_i + |J_i| - K}{2}S\ln(|S|-y)\Big|_{y_i}^{y_{i+1}} + KS\left\{\left[\arcsin\left(\frac{\sqrt{y}}{\sqrt{|S|}}\right) - \frac{\sqrt{y}}{\sqrt{|S|-y}}\right]\cdot\arcsin\left(\frac{\sqrt{y}}{\sqrt{|S|}}\right) - \frac{1}{2}\left[\arcsin\left(\frac{\sqrt{y}}{\sqrt{|S|}}\right)\right]^2\right\}\Big|_{y_i}^{y_{i+1}}.$$

Table 2. Analytical calculus steps of the $\int y\,\mathrm{d}x$ integral in the $w^2 + E < 0$ case.

The last integral at point III, which involves the arcsine function as the integrand, has been treated by applying the integration by parts formula.

References

Anderson, J. 2003 *Modern Compressible Flow with Historical Perspective*. McGrawHill.

Batchelor, G.K. 2000 *An Introduction to Fluid Dynamics*. Cambridge University Press.

Bejan, A. 2013 *Convection Heat Transfer*, 4th edn. John Wiley & Sons.

Bermudez, A., Lopez, X. & Vasquez-Cendon, M.E. 2017 Finite volume methods for multi-component Euler equations with source terms. *Comput. Fluids* **156**, 113–134.

Cavazzuti, M. & Corticelli, M. 2017 Numerical modelling of Fanno flows in micro-channels: a quasi-static application to air vents for plastic molding. *Therm. Sci. Engng Prog.* **2**, 43–56.

Cavazzuti, M., Corticelli, M.A. & Karayiannis, T.G. 2020 Compressible Fanno flows in micro-channels: an enhanced quasi-2D numerical model for turbulent flows. *Intl Commun. Heat Mass Transfer* **111**, article 104448.

Cheng, N.S. 2008 Formulas for friction factor in transitional regions. *ASCE J. Hydraul. Engng* **134** (9), 1357–1362.

Cioncolini, A., Scenini, F., Duff, J., Szolcek, M. & Curioni, M. 2016 Choked cavitation in micro-orifices: an experimental study. *Exp. Thermal Fluid Sci.* **74**, 49–57.

Douglas, J.F., Gasiorek, J.M., Swaffield, J.A. & Jack, L.B. 2005 *Fluid Mechanics*, 5th edn. Pearson Prentice Hall.

Dwight, H.B. 1961 *Tables of Integrals and Other Mathematical Data*. MacMillan Company.

Emmons, H.W. 1958 *Fundamentals of Gas Dynamics*. Princeton University Press.

Ferrari, A. 2021 Exact solutions for quasi one-dimensional compressible viscous flows in conical nozzles. *J. Fluid Mech.* **915**, A1.

Hairer, E., Norsett, S.P. & Wanner, G. 1993 *Solving Ordinary Differential Equations I. Nonstiff Problems*, 2nd edn. Springer-Verlag.

Hirsch, C. 2007 *Numerical Computation of Internal and External Flows*. Butterworth-Heinemann.

Kandlikar, S.G., Garimella, S., Li, D., Colin, S. & King, M.R. 2013 *Heat Transfer and Fluid Flow in Minichannels and Microchannels*. Butterworth-Heinemann.

Kirkland, W.M. 2019 A polytropic approximation of compressible flow in pipes with friction. *ASME Trans. J. Fluids Engng* **141** (12), article no. 121404.

Kumar, N.S. & Ooi, K.T. 2014 One dimensional model of an ejector with special attention to Fanno flow within the mixing chamber. *Appl. Thermal Engng* **65** (1), 226–235.

Laney, C. 1998 *Computational Gasdynamics*. Cambridge University Press.

Le Veque, R.J. 1990 *Numerical Methods for Conservation Laws*. Birkhauser Verlag.

Maeda, K. & Colonius, T. 2017 A source term approach for generation of one-way acoustic waves in the Euler and Navier–Stokes equations. *Wave Motion* **75**, 36–49.

Maicke, B.A. & Majdalani, J. 2012 Inversion of the fundamental thermodynamic equations for Isen-tropic nozzle flow analysis. *Trans. ASME: J. Engng Gas Turbines Power* **134**, 031201.

Mignot, G.P., Anderson, M.H. & Corradini, M.I. 2009 Measurement of supercritical CO_2 flow: effects of L/D and surface roughness. *Nucl. Engng Des.* **239** (5), 949–955.

Morimune, T., Hirayama, N. & Maeda, T. 1980*a* Study of compressible high-speed gas flow in piping system. 1st report, piping systems with bends or elbows. *Bull. JSME* **23** (186), 1997–2004.

Morimune, T., Hirayama, N. & Maeda, T. 1980*b* Study of compressible high-speed gas flow in piping system. 2nd report, piping systems with sudden enlargement. *Bull. JSME* **23** (186), 2005–2012.

Prud'homme, R. 2010 *Flows of Reactive Fluids*. Springer.

Rodriguez Lastra, M., Fernandez Oro, J.M., Vega Galdo, M., Marigorta Blanco, E. & Morros Santolaria, C. 2013 Novel design and experimental validation of a contraction nozzle for aerodynamic measurements in a subsonic wind tunnel. *J. Wind Engng Ind. Aerodyn.* **118**, 35–43.

Rosa, P., Karayiannis, T.G. & Collins, M.W. 2009 Single-phase heat transfer in micro-channels: the importance of scaling effects. *Appl. Therm. Engng Prog.* **29**, 3447–3468.

Shapiro, A. 1953 *The Dynamics and Thermodynamics of Compressible Fluid Flow*, vol. 1. John Wiley & Sons.

Sutton, G.P. 1992 *Rocket Propulsion Elements*, 6th edn. Wiley.

Tannehill, J.C., Anderson, D.A. & Pletcher, R.H. 1997 *Computational Fluid Mechanics and Heat Transfer*. Taylor and Francis.

Toro, E. 2009 *Riemann Solvers and Numerical Methods for Fluid Dynamics*. Springer-Verlag.

Urata, E. 2013 A flow-rate equation for subsonic Fanno flow. *Proc. Inst. Mech. Engrs* C **227** (12), 2724–2729.

WHITE, F.M. 2015 *Fluid Mechanics*, 8th edn. McGrawHill.
YARIN, L.P. 2012 *The Pi-Theorem - Applications to Fluid Mechanics and Heat and Mass Transfer*. Springer-Verlag.
YU, K., CHEN, Y., HUANG, S., LV, Z. & XU, J. 2020 Optimization and analysis of inverse design method of maximum thrust scramjet nozzles. *Aerosp. Sci. Technol.* **105**, article no. 105948.
ZUCKER, R.D. & BIBLARZ, O. 2002 *Fundamentals of Gasdynamics*. John Wiley & Sons.